

Exponential Reduction in Sample Complexity with Learning of Ising Model Dynamics

Arkopal Dutt¹ Andrey Y. Lokhov² Marc Vuffray² Sidhant Misra²

Abstract

The usual setting for learning the structure and parameters of a graphical model assumes the availability of independent samples produced from the corresponding multivariate probability distribution. However, for many models the mixing time of the respective Markov chain can be very large and i.i.d. samples may not be obtained. We study the problem of reconstructing binary graphical models from correlated samples produced by a dynamical process, which is natural in many applications. We analyze the sample complexity of two estimators that are based on the interaction screening objective and the conditional likelihood loss. We observe that for samples coming from a dynamical process far from equilibrium, the sample complexity reduces exponentially compared to a dynamical process that mixes quickly.

1. Introduction

A graphical model (GM) is a convenient description of a probabilistic distribution which highlights the structure of the conditional dependencies existing between a set of random variables. We focus our attention on GMs that can be expressed as elements of an exponential family and are naturally associated with a graph that captures the underlying structure of the conditional dependencies. These GMs, sometimes referred as positive Markov random fields or Boltzmann distributions, are ubiquitous tools used to describe behaviors of random systems across a broad range of sciences such as physics (Chaves et al., 2015), biology (Jansen et al.), medicine (Constantinou et al., 2016), data mining (Buczak & Guven, 2016) and computer vision (Wang et al., 2013). The expression of GMs can sometimes be deduced from first principles, but often it has to be learned from observed data accessible through

¹Research Laboratory of Electronics, Massachusetts Institute of Technology, Cambridge, MA, USA ²Theoretical Division, Los Alamos National Laboratory, Los Alamos, NM, USA. Correspondence to: Andrey Y. Lokhov <lokhover@lanl.gov>.

measurements and experiments. As these samples are time-consuming or costly to produce, it is not surprising that efficient GM learning methods play an important role in various fields such as in the study of gene expression (Marbach et al., 2012), protein interactions (Morcos et al., 2011), neuroscience (Schneidman et al., 2006a), image processing (Roth & Black, 2005), sociology (Eagle et al., 2009) and even grid science (He & Zhang, 2011).

The practical problem of learning a GM from observed data has a long-standing and rich history that can be traced back to the seminal work of Chow-Liu (Chow & Liu, 1968). However, it wasn't until recently and after further developments that a body of work showed one can efficiently reconstruct GMs from independent and identically distributed (i.i.d.) samples (Bresler, 2015; Vuffray et al., 2016; Hamilton et al., 2017; Klivans & Meka, 2017; Lokhov et al., 2018; Vuffray et al., 2019). In these papers, two methods stand out for being essentially optimal in the number of samples that they require (Lokhov et al., 2018). These methods are named Regularized Interaction Screening Estimator (RISE) and Regularized Pseudo-likelihood Estimator (RPLE) and both rely on the minimization of a convex loss function. The sample complexity of these estimators scales exponentially with a quantity named β that represents the maximum magnitude of the parameters in the GM. This exponential dependence in β is a fundamental limit of GM learning from i.i.d. samples (Santhanam & Wainwright, 2012) with heavy practical consequences as it restricts the possibility of learning GMs when data is scarce. However, the assumption of having access to independent samples is a modeling hypothesis that is convenient in many ways, but for which we can challenge the limits of its validity as it is known that sampling from arbitrary GMs is an NP-hard task. In most of the experimental settings mentioned earlier, the samples are actually obtained from a dynamic process whose stationary distribution is captured by a GM. Even the state of the art sampling techniques for GMs are implemented through Markov Chain Monte-Carlo (MCMC) dynamics (Levin & Peres, 2017; Gotovos et al., 2015). It is therefore natural to wonder if learning a graphical model from a dynamical process can be beneficial from a sample complexity standpoint.

Surprisingly, GM learning from dynamics has been rigor-

ously studied very little with the notable exception of the paper of Bresler, Gamarnik and Shah (Bresler et al., 2017). In an attempt to demonstrate that learning GMs from non-i.i.d. samples can be tractable, a question that was still widely debated at the time of the paper’s initial release, Bresler, Gamarnik and Shah proved that one can efficiently learn GMs using samples coming from Glauber dynamics (Glauber, 1963), an iconic MCMC sampling dynamics. This result was regrettably overshadowed by the progress made in the following years in GM learning and their algorithm suffers from an impractical scaling much worse compared to what one could obtain with RISE or RPLE in the i.i.d. sample setting. The question of whether correlated samples from dynamics can improve the sample complexity of GM learning remains unanswered.

A hint on the fact that such a reduction in sample complexity is possible is provided by a number of empirical studies in the statistical physics literature that considered reconstruction using mean-field methods (Roudi & Hertz, 2011; Mézard & Sakellariou, 2011; Zeng et al., 2011; Zhang, 2012; Bachschmid-Romano & Opper, 2015) and using pseudo-likelihood (Besag, 1975) based estimators (Zeng et al., 2013; Decelle & Zhang, 2015; Decelle et al., 2016) in various settings, although most of these studies focus on a simpler setting of asymmetric couplings known as kinetic Ising model that does not contain the GM as its equilibrium state. We do not consider mean-field based methods here because these methods are not exact and typically only work for high-temperature (weakly coupled) models, see (Lokhov et al., 2018) for an extensive discussion on the value of exact algorithms. Existing studies of pseudo-likelihood based estimators have been mostly conducted in a setting of reconstruction of single instances, and with a focus on parameter estimation (instead of structure learning for which the sample complexity bounds are known); hence, it is hard to extract the sample complexity scalings with model parameters such as β from these works. Still, single-instance reconstruction results indicate that in practice the number of samples required for an accurate model learning in the dynamic case seems to be significantly smaller compared to the i.i.d. learning setting.

In this work, we quantify through a carefully designed set of experiments and a rigorous mathematical analysis the reduction in sample complexity that one can achieve using samples from Glauber dynamics. We focus our attention on Ising models, the celebrated class of pairwise and binary GMs for which information-theoretic lower-bounds on sample complexity exist both for i.i.d. samples (Santhanam & Wainwright, 2012) and samples coming from Glauber dynamics (Bresler et al., 2017). We propose an adaptation of the efficient learning algorithms RISE and RPLE for learning GMs with dynamical samples; Interaction Screening method has never been previously considered for learning in

the dynamic setting. We extract the β scaling of the sample complexity for different instances of Ising models in two different dynamical regimes. The first, denoted as T-regime, consists in learning an Ising model from a single Glauber dynamic trajectory that mixes quickly toward its stationary distribution. The second, referred to as M-regime, consists in learning an Ising model from a series of one step evolutions of the Glauber dynamics from an initial distribution thus mimicking the trajectory of a system far from its mixed state. A similar setting of learning from a number of short trajectories starting with uniformly sampled configurations instead of one long trajectory has been considered in (Decelle et al., 2016). We find that the β scaling in the T-regime is similar to the one obtained from learning GMs with i.i.d. samples, an expected result since the Glauber dynamics produces i.i.d. samples once it has mixed. However, our main finding is that in the M-regime the β scaling depends crucially on the initial distribution, and for dynamics far from equilibrium we achieve a β exponent scaling up to ten times better than in the i.i.d. case. This exponential improvement in the sample complexity concretely translates into a reduction in sample requirements by a factor $10^4 - 10^5$ in typical regimes where variables of the GMs display non-trivial correlations. Our results also have a deep theoretical implication as we show that samples acquired far from the equilibrium carry more information about the structure of the problem. Based on this intuition, we design an active learning algorithm that modifies the trajectory of the dynamics on the fly to optimize the sample complexity of the learning task.

The paper is organized as follows. In Sec. 2, we define the problem of learning an Ising model from Glauber dynamics and describe two different regimes under which learning can take place. In Sec. 3, we present our learning algorithms and a theoretical analysis of their scaling properties. Additionally, we assess their performance experimentally on a variety of Ising models of different topologies and interaction strengths. In Sec. 4, we illustrate a real world application of our algorithms and present how active learning can be used to gain further advantage in learning from dynamics. The conclusion can be found in Sec. 5.

2. Problem statement

2.1. Ising model

Consider the Ising model on a graph $G = (V, E)$ with n nodes where $V = [n]$ is the set of nodes and $E \subset V \times V$ is the set of undirected edges. Each node $i \in V$ is associated with a spin which we will denote by σ_i and is a binary random variable taking values in $\{-1, +1\}$. The neighborhood of a node i is denoted by $\partial i = \{j \in V \mid (i, j) \in E\}$. The probability measure of a particular configuration of spins $\underline{\sigma} \in \{-1, +1\}^n$ is given by the Gibbs distribution

$$p(\underline{\sigma}) = \frac{1}{Z} \exp \left(\sum_{(i,j) \in E} J_{ij}^* \sigma_i \sigma_j + \sum_{i \in V} H_i^* \sigma_i \right), \quad (1)$$

where $\underline{J}^* = \{J_{ij}^*\}_{(i,j) \in E}$ is the vector of non-zero interactions associated with each edge, and $\underline{H}^* = \{H_i^*\}_{i \in V}$ is the vector of magnetic fields associated with each node. The normalization factor $Z = \sum_{\underline{\sigma}} \exp \left(\sum_{(i,j) \in E} J_{ij}^* \sigma_i \sigma_j + \sum_{i \in V} H_i^* \sigma_i \right)$ is referred to as the partition function and is in general NP-hard to compute (Sly & Sun, 2012).

2.2. Glauber dynamics and observations

Glauber dynamics is a reversible Markov chain that was originally introduced in (Glauber, 1963) for Ising models and can be generalized for any Markov random field. The Glauber dynamics is specified by the update rule that determines its transition probabilities. The spin configuration at any time t is denoted by $\underline{\sigma}^t$ with the initial configuration being $\underline{\sigma}^0$. At each time step t , a node is chosen uniformly at random. The corresponding random variable is given by I^{t+1} . Conditioned on $I^{t+1} = i$, the spin σ_i is updated according to the following conditional distribution:

$$p(\sigma_i^{t+1} | \underline{\sigma}^t) = \frac{\exp \left[\sigma_i^{t+1} \left(\sum_{j \in \partial i} J_{ij}^* \sigma_j^t + H_i^* \right) \right]}{2 \cosh \left[\sum_{j \in \partial i} J_{ij}^* \sigma_j^t + H_i^* \right]}. \quad (2)$$

The initial configuration $\underline{\sigma}^0$ is assumed to be drawn from some distribution $p_0(\underline{\sigma}^0)$. Executing m steps of the Glauber dynamics yields the samples $\underline{\sigma}^1, \underline{\sigma}^2, \dots, \underline{\sigma}^m$ and the corresponding sequence of node identities is then I^1, I^2, \dots, I^m . It can be used to draw i.i.d. samples from the Gibbs distribution in (1) when run long enough to allow for mixing. However, for a large class of models this mixing time is exponentially high (Martinelli & Olivieri, 1994), limiting its computational tractability. At the same time, many out-of-equilibrium natural systems such as biological neural networks naturally generate temporally correlated spike train data (Berry et al., 1997; Pillow et al., 2008) that is well described and is modeled by the Glauber dynamics (Marre et al., 2009; Tyrcha et al., 2013). This raises the problem of learning the graphical model associated with the sequence of time-correlated samples produced by Glauber dynamics, with the goals of inferring the connectivity of the system, predicting the final state of the dynamics, or for building a reliable model that can be used to simulate and predict the dynamics starting from other configurations.

2.3. Glauber dynamics with multi-start and the model selection problem

Suppose that the Glauber dynamics is run in batches of size m_r for $r = 1, \dots, R$ with total number of samples

$\sum_r m_r = m$. For each r , the initial configuration is picked according to the probability distribution p_0 and a sequence of m_r steps of the Glauber dynamics are executed to obtain m_r samples. In this paper, we consider two extreme cases. The **T-regime** corresponds to $R = 1$ and $m_1 = m$ where starting from an initial configuration, one batch of size m is executed to obtain m samples. The **M-regime** corresponds to $m_r = 1 \forall r$ and executing one step of the Glauber dynamics m times, each time starting from a new initial configuration. The two regimes are designed to emulate the behaviour of the Markov chain close to the equilibrium distribution (T-regime), and far from the equilibrium distribution (M-regime).

For stating sample complexity results, it is convenient to define a minimum non-zero coupling $\alpha = \min_{(i,j) \in E} |J_{ij}^*|$, the maximum coupling strength $\beta = \max_{(i,j) \in E} |J_{ij}^*|$, and a maximum nodal degree d for the Ising model in (1).

The dynamic model selection problem: Given m samples of spin configurations and corresponding node identities $\{(\underline{\sigma}^t, \underline{\sigma}^{t+1}, I^{t+1})\}_{t=0, \dots, m-1}$ observed from the Glauber dynamics from either the T-regime or M-regime, the model selection problem consists of two parts:

1. *Parameter estimation:* Compute estimates \hat{J}_{ij} of J_{ij}^* such that for all $1 \leq i, j \leq n$, we have $\|\hat{J}_{ij} - J_{ij}^*\| \leq \tilde{\alpha}/2$, where $\|\cdot\|$ is the norm of interest and $\tilde{\alpha}$ is the required precision.
2. *Structure reconstruction:* Compute an estimate \hat{E} of E such that the probability of perfect reconstruction satisfies $p[\hat{E} = E] \geq 1 - \delta$ where δ defines the confidence.

Most existing methods in the literature (Vuffray et al., 2016; 2019; Klivans & Meka, 2017) use parameter estimation to perform structure reconstruction. It is evident that whenever the parameters can be estimated with precision $\tilde{\alpha} = \alpha$, the structure estimated by the thresholding procedure given by

$$\hat{E}(\alpha) = \{1 \leq (i, j) \leq n \mid |\hat{J}_{ij}| \geq \alpha/2\}, \quad (3)$$

results in a perfect reconstruction with high probability. An information theoretic lower bound for the dynamic model selection problem from a single trajectory was derived in (Bresler et al., 2017) and is given by

$$m \geq \frac{e^{2\beta d/3}}{32d\alpha e^{d+3\beta+6}} n \log n \quad (4)$$

In comparison, the information-theoretic sample complexity for learning from i.i.d. samples (Santhanam & Wainwright, 2012) scales as $\exp(\beta d)$. It still remains unclear if either of the information theoretic lower bounds are tight. Current evidence or constructive proofs show a scaling of $\exp(4\beta d)$ for the i.i.d. case (Lokhov et al., 2018) and $\exp(20\beta d)$ for the general dynamic case (Bresler et al., 2017).

3. Learning Ising models from dynamics

3.1. Learning algorithms

We now describe how to adapt RISE and RPLE into computationally efficient estimators for learning Ising models from Glauber dynamics. Both algorithms minimize a convex loss function that relies on the properties of the conditional distributions rather than the full probability distribution. These methods reconstruct the neighborhoods of each node independently and are, therefore, fully parallelizable. Moreover, the minimization procedure can be implemented in $\tilde{O}(n^2)$ using entropic gradient descent for both RISE (Vuffray et al., 2019) and RPLE (see (Klivans & Meka, 2017) for a related stochastic first-order method with multiplicative updates).

Unlike the i.i.d. sample setting, the Glauber dynamics naturally takes the form of a local neighborhood update rule conditioned on the event that the spin i is updated, see Eq. (2). Following the construction of the RISE estimator in (Vuffray et al., 2016), we define the Dynamic Interaction Screening Objective for each node $i \in V$ as being the inverse of the exponent of the conditional distribution,

$$\begin{aligned} \mathbf{D\text{-}ISO:} \quad & \mathcal{S}_m(\underline{J}_i, H_i) \\ &= \frac{1}{m_i} \sum_{t=1}^m \exp \left[-\sigma_i^{t+1} \left(\sum_{j \neq i} J_{ij} \sigma_j^t + H_i \right) \right] \delta_{i, I^{t+1}}, \end{aligned} \quad (5)$$

where $\underline{J}_i := \{J_{ij} \mid j \neq i\} \in \mathbb{R}^{n-1}$ denotes the vector of pairwise interactions around a node i , and $m_i = \sum_{t=1}^m \delta_{i, I^{t+1}}$. The Kronecker delta $\delta_{i, I^{t+1}}$ in Eq. (5) is used to keep samples for which updates happened at i .

We call the corresponding estimator which uses D-ISO as the *Dynamic Regularized Interaction Screening Estimator (D-RISE)* and is defined in the spirit of (Vuffray et al., 2016) as the following convex program,

$$\mathbf{D\text{-}RISE:} \quad (\hat{J}_i, \hat{H}_i) = \operatorname{argmin}_{(\underline{J}_i, H_i)} \mathcal{S}_m(\underline{J}_i, H_i) + \lambda \|\underline{J}_i\|_1, \quad (6)$$

where the ℓ_1 -regularization promotes sparsity and λ is a tunable parameter controlling the amount of sparsity enforced.

The pseudo-likelihood based estimator can be understood as the (negative) conditional likelihood (Ravikumar et al., 2010) of an update at node i and takes the following form in the case of Glauber dynamics,

$$\begin{aligned} \mathbf{D\text{-}PL:} \quad & \mathcal{L}_m(\underline{J}_i, H_i) \\ &= -\frac{1}{m_i} \sum_{t=1}^m \ln \left[1 + \sigma_i^{t+1} \tanh \left(\sum_{j \neq i} J_{ij} \sigma_j^t + H_i \right) \right] \delta_{i, I^{t+1}}. \end{aligned} \quad (7)$$

Analogous to D-RISE, the *Dynamic Regularized Pseudo-Likelihood Estimator (D-RPLE)* takes the form of an ℓ_1 -

regularized convex program,

$$\mathbf{D\text{-}RPLE:} \quad (\hat{J}_i, \hat{H}_i) = \operatorname{argmin}_{(\underline{J}_i, H_i)} \mathcal{L}_m(\underline{J}_i, H_i) + \lambda \|\underline{J}_i\|_1 \quad (8)$$

The performance of the learning algorithms depends on the regularization parameter λ . Setting it too high encourages the interaction parameters to drop out and setting it too low can make the estimation sensitive to noise. Following theoretical considerations explained further, a good choice for successfully reconstructing the local neighborhood of i with probability $1 - \delta'$ (where $\delta' = \delta/n$ and $1 - \delta$ is the success of the whole graph reconstruction) is to set $\lambda = c_\lambda \sqrt{\log(n^2/\delta')/m_i}$ where the intensity of the penalty increases in a logarithmic fashion with the size of the system n and decreases with the number of spin updates observed m_i . The parameter $c_\lambda > 0$ is a numerical constant independent of the problem parameters such as m_i and n .

One of our main contributions is the following theorem which quantifies the sample complexity required for structure learning from Glauber dynamics in the M-regime.

Theorem 1 (M-regime: Structure Learning of Ising Model Dynamics). *Let $\{(\underline{\sigma}^t, \underline{\sigma}^{t+1}, I^{t+1})\}_{t=0, \dots, m-1}$ be m samples of spin configurations and corresponding node identities drawn through Glauber dynamics (Eq. 2), and define $m_i = \sum_{t=1}^m \delta_{i, I^{t+1}}$ as the number of updates per spin i . Consider M-regime on an Ising model with maximum degree d , maximum coupling intensity β , minimum coupling intensity α , and for simplicity assume $H_i^* = 0 \forall i$. Then for any $\delta > 0$, the following estimators with penalty parameter of form $\lambda \propto \sqrt{\log(3n^3/\delta)/m_i}$ reconstruct the edge-set perfectly with probability $p(\hat{E}(\lambda, \alpha) = E) \geq 1 - \delta$ if the number of samples satisfies*

- i) *D-RPLE: $m_i \geq C_d \max(1, \alpha^{-2}) \exp(4\beta d) \ln(3n^3/\delta)$,*
- ii) *D-RISE: $m_i \geq C'_d \max(1, \alpha^{-2}) \exp(2\beta d) \ln(3n^3/\delta)$,*

where C_d and C'_d depend only polynomially on d .

A more precise statement and proof of Theorem 1 is given in Appendix S1. Notice that given the choice of the initial distribution $p(\underline{\sigma}_0)$ to be the uniform distribution, the total number of samples m required to get the number of samples m_i that satisfies Theorem 1 is $m = O(n m_i)$. Notice that unlike the i.i.d. case where the entire sample may be distinct, in the dynamic case only a single spin is updated while the values of other variables are kept fixed; hence, perhaps a more natural quantity for comparison with the i.i.d. case is the number of updates per spin m_i instead of m .

We expect the worst-case scalings of learning from dynamics in the T-regime to be similar to the i.i.d. setting as it includes the fully mixed setting as a particular case. The main contribution of Theorem 1 lies in that it establishes

with certainty that the scaling of D-RISE in the M-regime is strictly better than in the i.i.d. setting where it was found experimentally to be at least $\exp(4\beta d)$ in the worst case (Lokhov et al., 2018). It is also interesting to compare the above results to the theoretical analysis of the i.i.d. setting for which RPLE and RISE have scalings upper-bounded by $\exp(8\beta d)$ and $\exp(6\beta d)$ respectively (Lokhov et al., 2018). However, these theoretical upper-bounds tend to be loose and this motivates us to quantify the scalings achieved in practice in the dynamic case experimentally.

3.2. Empirical β scaling of the sample complexity

Our main goal is to assess the empirical sample complexity of our learning algorithms in both the T-regime and M-regime. In particular, we want to extract the exponential scaling of the sample complexity for successful structure reconstruction with respect to β , the magnitude of the largest coupling. The sample complexity of D-RPLE and D-RISE are tested over Ising models of different topologies and interaction strengths. We do not include a comparison to the algorithm of (Bresler et al., 2017) due to its high computational complexity, and to heuristic mean-field methods (Roudi & Hertz, 2011; Mézard & Sakellariou, 2011; Zeng et al., 2011; Zhang, 2012; Bachschmid-Romano & Opper, 2015) since most of them are derived for asymmetric kinetic Ising model, and are not guaranteed to reconstruct arbitrary strongly interacting models; instead, we focus on studying the performance of two exact methods that can be efficiently implemented through convex optimization.

We denote the minimal number of samples required for perfect structure reconstruction with probability $1 - \delta \geq 0.95$ (for $\delta = 0.05$) as m^* . Our experimental protocol to find m^* (sample complexity of the structure learning problem) is similar to the one from Supplementary material of (Lokhov et al., 2018). For each graphical model topology and coupling values, we determined m^* by finding the minimal value of m samples required to successively reconstruct the structure 45 times in a row from 45 independent sets of m samples, which guarantees a 90% confidence for $\delta = 0.05$.

We reconstruct the topology by first solving the optimization problems in Eq. (6) for D-RISE and in Eq. (8) for D-RPLE with appropriate ℓ_1 regularization to obtain estimates of (\hat{J}_i, \hat{H}_i) at each node $i \in V$. We create a consensus of the estimated couplings by averaging the reconstruction from two nodes i.e. $\hat{J}_{ij}^{\text{avg}} = (\hat{J}_{ij} + \hat{J}_{ji})/2$. The set of pairwise interactions \hat{J}^{avg} which are higher than $\alpha/2$ are defined as the estimate of the edge set \hat{E} . The structure is declared to be successfully reconstructed when the edge set is perfectly recovered $\hat{E} = E$.

We perform an extensive set of numerical experiments to empirically obtain m^* for a variety of graphs in both the

T-regime and the M-regime. We consider two different topologies: the periodic two-dimensional lattice and the random 3-regular graph. Each of these two topologies are subdivided into three categories according to the signs of the interaction couplings. This includes the ferromagnetic case with positive couplings, the spin glass case with couplings taking random signs and the ferromagnetic case with a weak anti-ferromagnetic impurity (i.e., weak negative coupling). For each of these six cases, all the couplings' magnitudes are set to $|J_{ij}^*| = \beta$ with exception of one or two couplings which are set to $|J_{ij}^*| = \alpha$. In our experiments, we fixed the value of $\alpha = 0.4$ and varied β from α to a value ranging from 1 to 4 depending on the model. All models have their magnetic fields at each node H_i^* set to zero. These cases are identical to the test cases used in (Lokhov et al., 2018) in the i.i.d. learning setting which enables us to draw a comparison between the dynamic and i.i.d. settings.

In deciding the ℓ_1 -regularization to be used, optimal values of c_λ which are unknown a priori were determined through detailed numerical simulations on different Ising model topologies as described in Appendix S3. The determined optimal values of c_λ are summarized in Table 1 on lattices and random regular (RR) graphs for the two different regimes.

	T-regime		M-regime	
	D-RISE	D-RPLE	D-RISE	D-RPLE
Lattices	0.1	0.05	0.1	0.05
RR Graphs	0.45	0.1	0.7	0.3

Table 1: Optimal values of c_λ for D-RISE and D-RPLE.

Our sample complexity results for the T-regime and M-regime are shown in Figure 1a and Figure 1b respectively. In the T-regime, the worst scalings of sample complexity are observed for both D-RISE and D-RPLE in lattices with purely ferromagnetic interactions (Fig. 1aA) and those with a weak anti-ferromagnetic interaction (Fig. 1aE). The worst cases are $\exp(4.2\beta d)$ and $\exp(4.5\beta d)$ for D-RISE and D-RPLE respectively. The scaling of sample complexity results are similar to the i.i.d. setting for the ferromagnetic models on lattices and random regular graphs. However, compared to the i.i.d. case, we obtain a 35% reduction in the β scaling for D-RISE for the spin glass model on a lattice and around 27% reduction for the spin glass model on a random regular graph. For the systems studied here, the Glauber dynamics mixes rapidly in the case of ferromagnetic models as the number of variables is small compared to the number of samples required to learn the structure. Therefore the dynamics in the T-regime quickly produces samples that behave like i.i.d. samples in these cases and we see similar scalings. This mixing may not be as rapid in the case of spin glass models, yielding us savings in number of samples when learning from Glauber dynamics.

The picture drastically changes as we move to the M-regime for which the scaling results are shown in Fig. 1b. Among

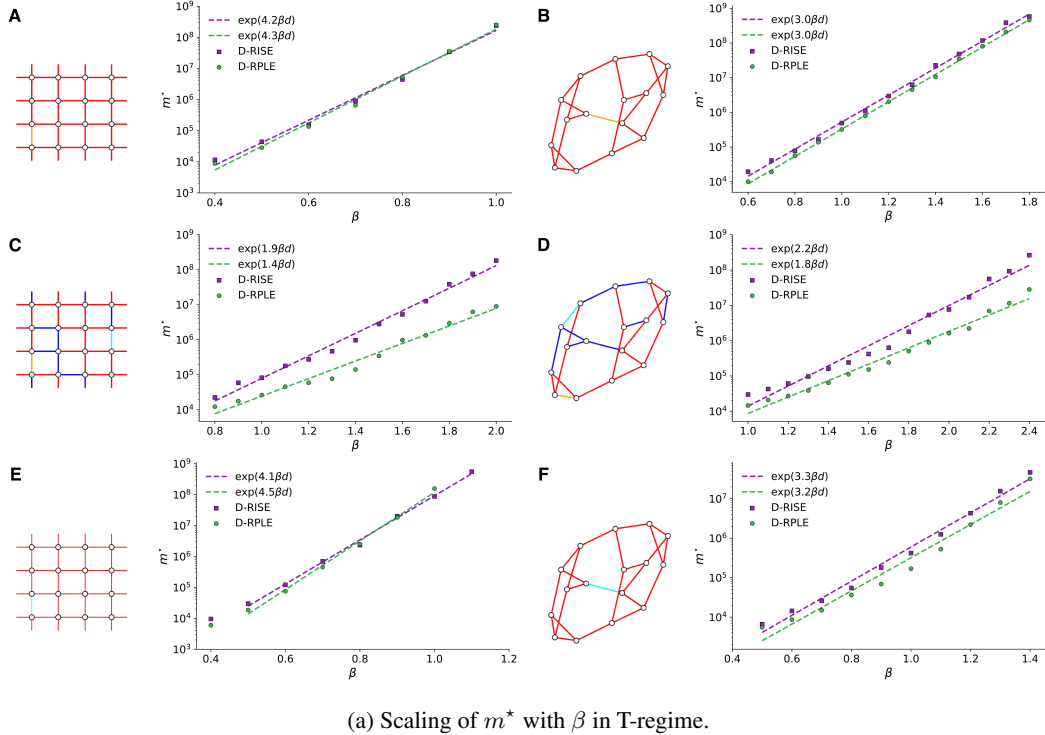
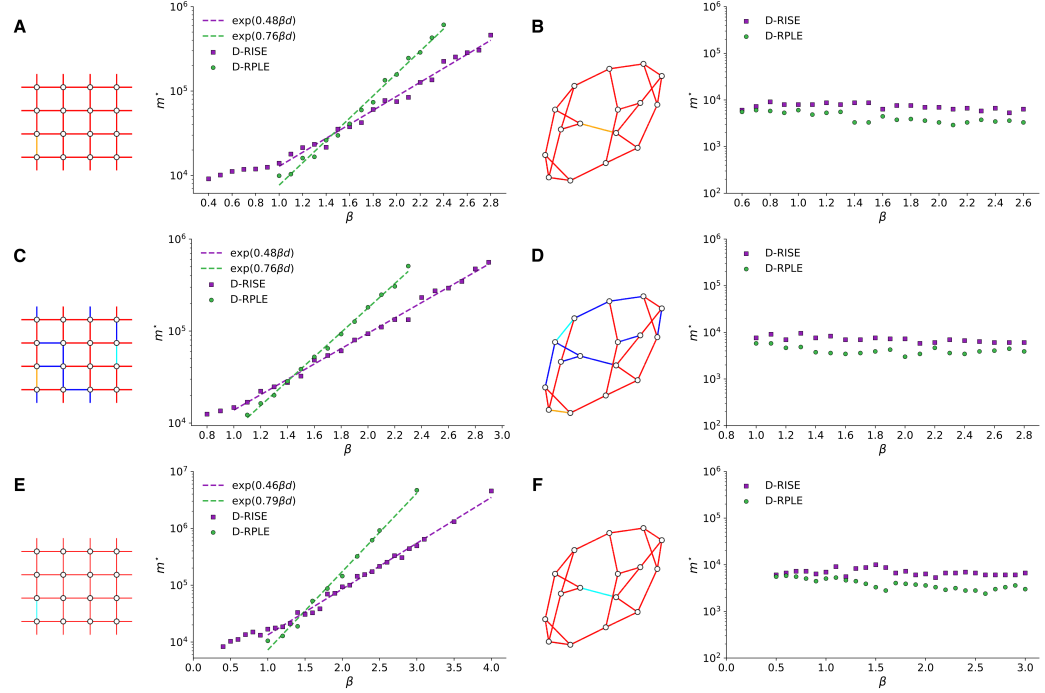

 (a) Scaling of m^* with β in T-regime.

 (b) Scaling of m^* with β in M-regime.

Figure 1: We assess the performance of D-RISE and D-RPLE in reconstructing Ising models of size $n = 16$ from samples generated from Glauber dynamics. The different Ising model topologies with their corresponding pictorial representations on the left-hand side of each plot are: (A) ferromagnetic model on a periodic lattice, (B) spin glass model on a periodic lattice, and (C) ferromagnetic model on a periodic lattice with weak antiferromagnetic impurity. Edges in the pictorial representations of the models are colored red (β), orange (α), cyan ($-\alpha$) and blue ($-\beta$). Value of $\alpha = 0.4$ for all the graphs.

the numerical examples that we consider, the worst-case scaling for D-RISE and D-RPLE observed are $\exp(0.48\beta d)$ and $\exp(0.79\beta d)$ respectively, with the scalings being very similar for all the lattices. Compared to the T-regime there is a reduction in the β scaling between 80% and 90%, translating to a reduction in the sample requirement of orders of magnitude. Interestingly, we observe that a constant number of samples independent of β is required for learning the random regular graphs. Thus, it is possible to beat exponential scalings for special topologies in the case of M-regime which would not be possible in the i.i.d. setting. The details of this behavior is described in Appendix S4.

The fundamental difference between the two regimes is that the Glauber dynamics comes effectively from two different initial distributions. In the M-regime, the samples are produced from a one step Glauber dynamics initialized with a uniform distribution. In the T-regime, however, the samples are *effectively* produced from a one step Glauber dynamics that is initialized from a distribution which is close to the equilibrium one, as the actual dynamics mixes more rapidly. This shows that the dynamical samples acquired far from the equilibrium carry more information about the structure of graphical models. A natural question to ask is then how to empirically find such an initial distribution for the Glauber dynamics that improves the sample complexity. We propose a possible solution to this issue by introducing an active learner in Section 4.2.

4. Applications

In this section, we illustrate how D-RISE/D-RPLE can be applied to a real world system and extended to improve their performance. In Section 4.1, we consider a multi-neuron spike trains' data set to learn the structure of a network of neurons. This can be used to understand the dynamics of the network and how it implements computations. In Section 4.2, we highlight an approach to modify the initial distribution to the M-regime to improve sample complexity.

4.1. Learning Ising models from neural data

Due to the high dimensionality of the space of spike patterns and lack of enough data to build an exact statistical description, it has become popular to use parametric models such as Ising models (Schneidman et al., 2006b). In the corresponding Ising model (Rieke et al., 1999), the spin σ_i of neuron/node i can be interpreted as spiking/firing ($\sigma_i = 1$) or not ($\sigma_i = -1$). Studies on using Ising models for spike trains include application to larger populations of neurons (Cocco et al., 2009; Nirenberg & Victor, 2007), conditions under which Ising models are good approximations (Roudi et al., 2009a; Tkacik et al., 2009), development of faster learning methods (Broderick et al., 2007) and comparisons of different learning methods (Roudi et al., 2009b). Most of

previous studies consider the i.i.d. setting. However, (Hertz et al., 2011) showed that respecting correlations in time and the dynamics can lead to better Ising model fits to the data. This motivates us to investigate the underlying Ising model for spike trains considering Glauber dynamics.

We consider the dataset from (Prentice et al., 2016) containing spike trains from 152 salamander retinal ganglion cells in response to a non-repeated natural movie stimulus, of which we select spike trains over $n = 42$ neurons over 24s for our application. To use D-RISE/D-RPLE, the dataset is first converted into a sequence of 1.2×10^5 spin configurations, a segment of which is shown as a spike raster in Figure 2. Time series of spin configurations along with updated node identities are then extracted from this sequence and 3.2×10^4 samples corresponding to the M-regime with an unknown initial distribution are obtained. Details of this procedure is given in Appendix S5.

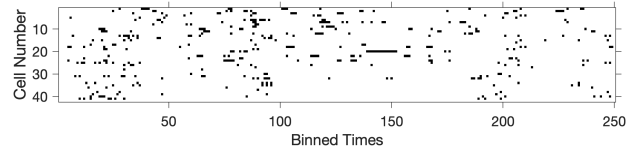


Figure 2: Spike raster from the first 5 sec of the data over 42 neurons. Each column indicates the spiking pattern of the neurons over a 20 ms time bin.

We discuss the statistics of Ising model parameters learned using D-RISE on this set of samples in Appendix S5, where we also compare the recovered parameters with those obtained by RISE assuming the samples are i.i.d. Correlations computed from data assuming the samples are i.i.d. (Figure 3a) and that respecting time (Figure 3b) are very different. This difference strengthens the importance of respecting dynamics when learning an effective Ising model if one would like to capture time correlations present in the data. The correlation matrix predicted using the model learned with D-RISE is presented in Figure 3c, and is within $\sim 10\%$ of that computed from data under the Frobenius norm (see Figure 3d), indicating a good model fit that respects the time correlations present in the data. Details of correlation computation can be found in the Appendix S5.

As we have control in such biological systems through external stimuli, learning an effective Ising model could be accelerated using an active learner which we discuss next.

4.2. Active learning in M-regime

Motivated by the previous section, we develop an active learning algorithm that optimizes on the fly over the initial distribution in the M-regime. In the M-regime, the initial spin configuration $\underline{\sigma}^0$ can be viewed as a query to the Glauber dynamics which returns the output of $(\underline{\sigma}^1, I^1)$.

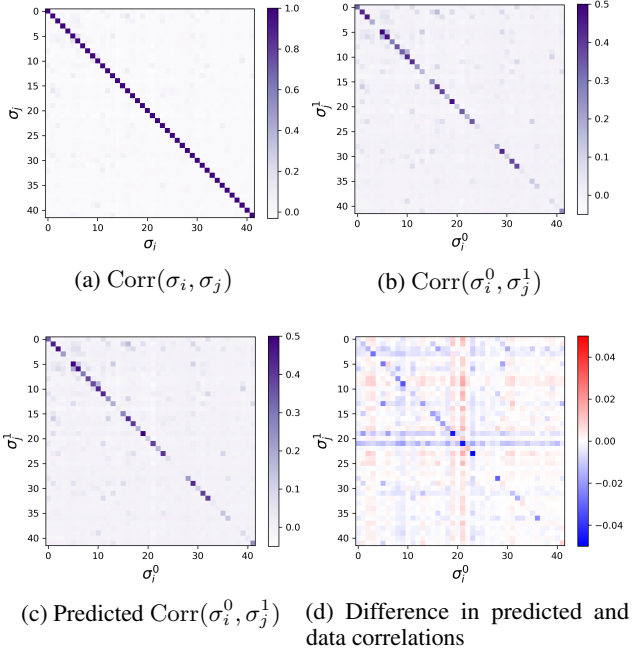


Figure 3: Correlation matrices are computed from data in (a) assuming the spin configurations are i.i.d., and (b) respecting time. We show the predicted correlation matrix using D-RISE estimates in (c) and its difference from that computed from data in (d).

Clearly, the observations generated have a dependence on the query distribution $p_{\underline{\sigma}^0}$ from which the queries $\underline{\sigma}^0$ are simulated. If no prior information about the parameter set $(\underline{J}, \underline{H})$ is known, then a suitable choice of $p_{\underline{\sigma}^0}$ is the uniform distribution over $\{-1, +1\}^n$ as we had chosen for our numerical experiments in the previous section.

In *active learning*, the learner has the ability to select queries during model learning that would be most informative. Here, we consider a *mini-batch adaptive active learning* (Wei et al., 2015) scheme where in each round a mini-batch of initial spin configurations $\underline{\sigma}^0$ are selected to be queried and then the samples obtained are combined with those from before to produce estimates of $(\underline{J}, \underline{H})$. These estimates are then used to determine the next mini-batch of queries. To select these queries we use the informative measure of entropy as in uncertainty sampling. An alternate criteria that can be used is Fisher information but the computational effort of the resulting query optimization typically grows exponentially with n (Sourati et al., 2017a). In uncertainty sampling (Settles, 2009), one query $\underline{\sigma}^0$ is chosen at a time

$$\hat{\underline{\sigma}}^0 = \underset{\underline{\sigma}^0 \in \{-1, +1\}^n}{\operatorname{argmax}} S(\underline{\sigma}^1 | \underline{\sigma}^0; \underline{J}, \underline{H}) \quad (9)$$

where S is the entropy measure of the probability $p(\underline{\sigma}^1 | \underline{\sigma}^0; \underline{J}, \underline{H})$ based on current parameter estimates. The

entropy in the case of Glauber dynamics is

$$S(\underline{\sigma}^1 | \underline{\sigma}^0) = \sum_{k \in [n]} \log(2 \cosh(A_k)) - A_k \tanh(A_k) \quad (10)$$

where $A_k = \sum_{l \in \partial k} J_{kl} \sigma_l^0 + H_k$. Here, we issue mini-batches of queries sampled from distribution q that is proportional to the the entropy S . Our algorithm is given in Algorithm 1.

Algorithm 1 Active Learning of Glauber Dynamics

Input: Initial set of samples $X^{(0)}$, number of mini-batches i_{max} , size of mini-batch m_b
 $(\underline{J}, \underline{H}) \leftarrow \text{D-RISE}(X^{(0)})$
for $i = 1 : i_{max}$ **do**
 Compute entropy $S(\underline{\sigma}^1 | \underline{\sigma}^0; \underline{J}, \underline{H}) \forall \underline{\sigma}^0$
 Set $q(\underline{\sigma}^0) \propto S(\underline{\sigma}^1 | \underline{\sigma}^0; \underline{J}, \underline{H})$
 Modify distribution: $q = \mu q + (1 - \mu) p_U$
 Sample m_b queries from $\{-1, +1\}^n$ w.p. q
 Obtain corresponding samples X_b by running Glauber dynamics in M-regime
 Set $X^{(i)} = X^{(i-1)} \cup X_b$
 $(\underline{J}, \underline{H}) \leftarrow \text{D-RISE}(X^{(i)})$
end for
Output: $(\underline{J}, \underline{H})$

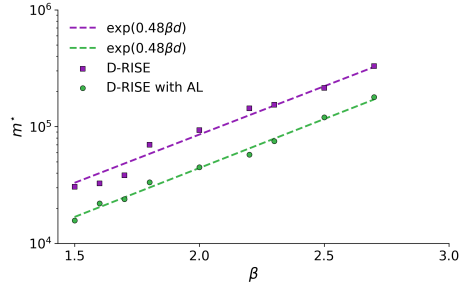


Figure 4: Scaling of m^* with β in M-regime. Performance comparison of D-RISE with active learning against a vanilla D-RISE in reconstructing a ferromagnetic model with weak anti-ferromagnetic impurity of size $n = 16$ (see Fig. 1bE).

Note that we slightly modify the query distribution q for each mini-batch by mixing it with the uniform distribution p_U . The mixing coefficient $0 \leq \mu \leq 1$ typically depends on the number of samples so far. We set it to $\mu = 1 - 1/|X^{(i)}|^{1/6}$ which is often used for such active learning algorithms (Sourati et al., 2017b; Chaudhuri et al., 2015).

To determine the sample complexity, the minimal number of samples required for successful structure reconstruction m^* is determined as described in Sec. 3.2. However, here each trial corresponds to an independent active learning run. In each trial for a given value of m , we consider the size of initial set of samples to be $\lfloor m/3 \rfloor$ and size of batches m_b such that there are a total of 15 mini-batches.

In Figure 4, we compare the sample complexity of D-RISE with and without active learning (AL) on the challenging

case of a ferromagnetic periodic lattice with a weak anti-ferromagnetic impurity (Fig. 1bE). We consider values of β between 1.5 and 2.7. While the scaling of sample complexity with β remains unchanged (within experimental error), there is about 47% reduction in the number of samples required for successful graph reconstruction when using AL.

5. Conclusions and future work

In this paper, we theoretically and empirically establish a fundamental difference between learning graphical models in the traditional framework of i.i.d. samples and samples obtained from out of equilibrium dynamics. We show that in the latter understudied setting, there is considerable improvement in sample complexity which has both theoretical and practical consequences. The code for the learning algorithms, active learner and data in this work is available upon request. In future work, it would be interesting to further investigate general Markov Random Fields and other Markov chain dynamics.

Acknowledgements

A.D. was partially supported by the Applied Machine Learning Fellowship at LANL where most of the work was carried out. A.Y.L., M.V., and S.M. acknowledge support from the Laboratory Directed Research and Development program of Los Alamos National Laboratory under project numbers 20190059DR, 20200121ER, and 20210078DR.

References

Acharya, J., Bhattacharyya, A., and Kamath, P. Improved bounds for universal one-bit compressive sensing. In *2017 IEEE International Symposium on Information Theory (ISIT)*, pp. 2353–2357, 2017. doi: 10.1109/ISIT.2017.8006950.

Bachschmid-Romano, L. and Opper, M. Learning of couplings for random asymmetric kinetic ising models revisited: random correlation matrices and learning curves. *Journal of Statistical Mechanics: Theory and Experiment*, 2015(9):P09016, 2015.

Beck, A. and Teboulle, M. Mirror descent and nonlinear projected subgradient methods for convex optimization. *Operations Research Letters*, 31(3):167–175, 2003.

Ben-Tal, A., Margalit, T., and Nemirovski, A. The ordered subsets mirror descent optimization method with applications to tomography. *SIAM Journal on Optimization*, 12(1):79–108, 2001.

Berry, M. J., Warland, D. K., and Meister, M. The structure and precision of retinal spike trains. *Proceedings of the National Academy of Sciences*, 94(10):5411–5416, 1997.

Besag, J. Statistical analysis of non-lattice data. *Journal of the Royal Statistical Society: Series D (The Statistician)*, 24(3):179–195, 1975.

Biegler, L. T. and Zavala, V. M. Large-scale nonlinear programming using ipopt: An integrating framework for enterprise-wide dynamic optimization. *Computers & Chemical Engineering*, 33(3):575–582, 2009.

Boufounos, P. T. and Baraniuk, R. G. 1-bit compressive sensing. In *2008 42nd Annual Conference on Information Sciences and Systems*, pp. 16–21, 2008. doi: 10.1109/CISS.2008.4558487.

Bresler, G. Efficiently learning Ising models on arbitrary graphs. In *Proceedings of the Forty-Seventh Annual ACM on Symposium on Theory of Computing*, pp. 771–782. ACM, 2015.

Bresler, G., Gamarnik, D., and Shah, D. Learning graphical models from the glauber dynamics. *IEEE Transactions on Information Theory*, 64(6):4072–4080, 2017.

Broderick, T., Dudik, M., Tkacik, G., Schapire, R. E., and Bialek, W. Faster solutions of the inverse pairwise ising problem. *arXiv preprint arXiv:0712.2437*, 2007.

Buczak, A. L. and Guven, E. A survey of data mining and machine learning methods for cyber security intrusion detection. *IEEE Communications Surveys Tutorials*, 18(2):1153–1176, 2016.

Chaudhuri, K., Kakade, S. M., Netrapalli, P., and Sanghavi, S. Convergence rates of active learning for maximum likelihood estimation. In *Advances in Neural Information Processing Systems*, pp. 1090–1098, 2015.

Chaves, R., Majenz, C., and Gross, D. Information-theoretic implications of quantum causal structures. *Nature communications*, 6:5766, 2015.

Chow, C. and Liu, C. Approximating discrete probability distributions with dependence trees. *IEEE Transactions on Information Theory*, 14(3):462–467, May 1968. ISSN 1557-9654. doi: 10.1109/TIT.1968.1054142.

Cocco, S., Leibler, S., and Monasson, R. Neuronal couplings between retinal ganglion cells inferred by efficient inverse statistical physics methods. *Proceedings of the National Academy of Sciences*, 106(33):14058–14062, 2009.

Constantinou, A. C., Fenton, N., Marsh, W., and Radlinski, L. From complex questionnaire and interviewing data to intelligent bayesian network models for medical decision support. *Artificial intelligence in medicine*, 67:75–93, 2016.

Decelle, A. and Zhang, P. Inference of the sparse kinetic ising model using the decimation method. *Physical Review E*, 91(5):052136, 2015.

Decelle, A., Ricci-Tersenghi, F., and Zhang, P. Data quality for the inverse Ising problem. *Journal of Physics A: Mathematical and Theoretical*, 49(38):384001, 2016.

Eagle, N., Pentland, A. S., and Lazer, D. Inferring friendship network structure by using mobile phone data. *Proceedings of the National Academy of Sciences*, 106(36):15274–15278, 2009. doi: 10.1073/pnas.0900282106.

Glauber, R. J. Time-dependent statistics of the Ising model. *Journal of mathematical physics*, 4(2):294–307, 1963.

Gotovos, A., Hassani, H., and Krause, A. Sampling from probabilistic submodular models. In Cortes, C., Lawrence, N. D., Lee, D. D., Sugiyama, M., and Garnett, R. (eds.), *Advances in Neural Information Processing Systems 28*, pp. 1945–1953. Curran Associates, Inc., 2015.

Hamilton, L., Koehler, F., and Moitra, A. Information theoretic properties of Markov random fields, and their algorithmic applications. In Guyon, I., Luxburg, U. V., Bengio, S., Wallach, H., Fergus, R., Vishwanathan, S., and Garnett, R. (eds.), *Advances in Neural Information Processing Systems 30*, pp. 2463–2472. Curran Associates, Inc., 2017.

He, M. and Zhang, J. A dependency graph approach for fault detection and localization towards secure smart grid. *IEEE Transactions on Smart Grid*, 2(2):342–351, June 2011. ISSN 1949-3053. doi: 10.1109/TSG.2011.2129544.

Hertz, J., Roudi, Y., and Tyrcha, J. Ising models for inferring network structure from spike data. *arXiv preprint arXiv:1106.1752*, 2011.

Jansen, R., Yu, H., Greenbaum, D., Kluger, Y., Krogan, N. J., Chung, S., Emili, A., Snyder, M., Greenblatt, J. F., and Gerstein, M. A Bayesian networks approach for predicting protein-protein interactions from genomic data. *302(5644):449–453*.

Kahn, J., Komlós, J., and Szemerédi, E. On the probability that a random ± 1 -matrix is singular. *Journal of the American Mathematical Society*, 8(1):223–240, 1995.

Klivans, A. and Meka, R. Learning graphical models using multiplicative weights. In *2017 IEEE 58th Annual Symposium on Foundations of Computer Science (FOCS)*, pp. 343–354, Oct 2017.

Levin, D. A. and Peres, Y. *Markov chains and mixing times*, volume 107. American Mathematical Soc., 2017.

Lokhov, A. Y., Vuffray, M., Misra, S., and Chertkov, M. Optimal structure and parameter learning of Ising models. *Science advances*, 4(3):e1700791, 2018.

Marbach, D., Costello, J. C., Kuffner, R., Vega, N. M., Prill, R. J., Camacho, D. M., Allison, K. R., Kellis, M., Collins, J. J., and Stolovitzky, G. Wisdom of crowds for robust gene network inference. *Nat Meth*, 9(8):796–804, Aug 2012. ISSN 1548-7091. doi: 10.1038/nmeth.2016.

Marre, O., El Boustani, S., Frégnac, Y., and Destexhe, A. Prediction of spatiotemporal patterns of neural activity from pairwise correlations. *Physical review letters*, 102(13):138101, 2009.

Martinelli, F. and Olivieri, E. Approach to equilibrium of Glauber dynamics in the one phase region. *Communications in Mathematical Physics*, 161(3):447–486, 1994.

Mézard, M. and Sakellariou, J. Exact mean-field inference in asymmetric kinetic Ising systems. *Journal of Statistical Mechanics: Theory and Experiment*, 2011(07):L07001, 2011.

Morcos, F., Pagnani, A., Lunt, B., Bertolino, A., Marks, D. S., Sander, C., Zecchina, R., Onuchic, J. N., Hwa, T., and Weigt, M. Direct-coupling analysis of residue coevolution captures native contacts across many protein families. *Proceedings of the National Academy of Sciences*, 108(49):E1293–E1301, 2011. doi: 10.1073/pnas.1111471108.

Negahban, S., Yu, B., Wainwright, M. J., and Ravikumar, P. K. A unified framework for high-dimensional analysis of m -estimators with decomposable regularizers. In *Advances in neural information processing systems*, pp. 1348–1356. Citeseer, 2009.

Nirenberg, S. H. and Victor, J. D. Analyzing the activity of large populations of neurons: how tractable is the problem? *Current opinion in neurobiology*, 17(4):397–400, 2007.

Pillow, J. W., Shlens, J., Paninski, L., Sher, A., Litke, A. M., Chichilnisky, E., and Simoncelli, E. P. Spatio-temporal correlations and visual signalling in a complete neuronal population. *Nature*, 454(7207):995–999, 2008.

Prentice, J. S., Marre, O., Ioffe, M. L., Loback, A. R., Tkačik, G., and Berry, M. J. Error-robust modes of the retinal population code. *PLoS computational biology*, 12(11):e1005148, 2016.

Ravikumar, P., Wainwright, M. J., Lafferty, J. D., et al. High-dimensional Ising model selection using ℓ_1 -regularized logistic regression. *The Annals of Statistics*, 38(3):1287–1319, 2010.

Rieke, F., Warland, D., Van Steveninck, R. D. R., Bialek, W. S., et al. *Spikes: exploring the neural code*, volume 7. MIT press Cambridge, 1999.

Roth, S. and Black, M. J. Fields of experts: a framework for learning image priors. In *Computer Vision and Pattern Recognition, 2005. CVPR 2005. IEEE Computer Society Conference on*, volume 2, pp. 860–867 vol. 2, June 2005. doi: 10.1109/CVPR.2005.160.

Roudi, Y. and Hertz, J. Mean field theory for nonequilibrium network reconstruction. *Physical review letters*, 106(4): 048702, 2011.

Roudi, Y., Nirenberg, S., and Latham, P. E. Pairwise maximum entropy models for studying large biological systems: when they can work and when they can't. *PLoS Comput Biol*, 5(5):e1000380, 2009a.

Roudi, Y., Tyrcha, J., and Hertz, J. Ising model for neural data: model quality and approximate methods for extracting functional connectivity. *Physical Review E*, 79(5): 051915, 2009b.

Santhanam, N. P. and Wainwright, M. J. Information-theoretic limits of selecting binary graphical models in high dimensions. *IEEE Transactions on Information Theory*, 58(7):4117–4134, 2012.

Schneidman, E., Berry, M. J., Segev, R., and Bialek, W. Weak pairwise correlations imply strongly correlated network states in a neural population. *Nature*, 440 (7087):1007–1012, Apr 2006a. ISSN 0028-0836. doi: 10.1038/nature04701.

Schneidman, E., Berry, M. J., Segev, R., and Bialek, W. Weak pairwise correlations imply strongly correlated network states in a neural population. *Nature*, 440(7087): 1007–1012, 2006b.

Settles, B. Active learning literature survey. Technical report, University of Wisconsin-Madison Department of Computer Sciences, 2009.

Sly, A. and Sun, N. The computational hardness of counting in two-spin models on d-regular graphs. In *2012 IEEE 53rd Annual Symposium on Foundations of Computer Science*, pp. 361–369. IEEE, 2012.

Sourati, J., Akcakaya, M., Erdogan, D., Leen, T. K., and Dy, J. G. A probabilistic active learning algorithm based on fisher information ratio. *IEEE transactions on pattern analysis and machine intelligence*, 40(8):2023–2029, 2017a.

Sourati, J., Akcakaya, M., Leen, T. K., Erdogan, D., and Dy, J. G. Asymptotic analysis of objectives based on fisher information in active learning. *The Journal of Machine Learning Research*, 18(1):1123–1163, 2017b.

Tkacik, G., Schneidman, E., Berry II, M. J., and Bialek, W. Spin glass models for a network of real neurons. *arXiv preprint arXiv:0912.5409*, 2009.

Tyrcha, J., Roudi, Y., Marsili, M., and Hertz, J. The effect of nonstationarity on models inferred from neural data. *Journal of Statistical Mechanics: Theory and Experiment*, 2013(03):P03005, 2013.

Vuffray, M., Misra, S., Lokhov, A., and Chertkov, M. Interaction screening: Efficient and sample-optimal learning of ising models. In *Advances in Neural Information Processing Systems*, pp. 2595–2603, 2016.

Vuffray, M., Misra, S., and Lokhov, A. Y. Efficient learning of discrete graphical models. *arXiv preprint arXiv:1902.00600*, 2019.

Wang, C., Komodakis, N., and Paragios, N. Markov random field modeling, inference & learning in computer vision & image understanding: A survey. *Computer Vision and Image Understanding*, 117(11):1610 – 1627, 2013. ISSN 1077-3142. doi: <https://doi.org/10.1016/j.cviu.2013.07.004>.

Wei, K., Iyer, R., and Bilmes, J. Submodularity in data subset selection and active learning. In *International Conference on Machine Learning*, pp. 1954–1963, 2015.

Zeng, H.-L., Aurell, E., Alava, M., and Mahmoudi, H. Network inference using asynchronously updated kinetic ising model. *Physical Review E*, 83(4):041135, 2011.

Zeng, H.-L., Alava, M., Aurell, E., Hertz, J., and Roudi, Y. Maximum likelihood reconstruction for ising models with asynchronous updates. *Physical review letters*, 110 (21):210601, 2013.

Zhang, P. Inference of kinetic ising model on sparse graphs. *Journal of Statistical Physics*, 148(3):502–512, 2012.

S1. Analysis of the estimators D-RISE and D-RPLE

In this section, we provide a rigorous analysis of the sample complexity of learning from Glauber dynamics in the M-regime on Ising models using the estimators of D-RISE and D-RPLE. Theorems 2 and 3 are established.

To simplify the analysis, we consider the case of Ising models with zero local magnetic fields (i.e., $H_i^* = 0$). The probability measure of a particular configuration of spins $\underline{\sigma} \in \{-1, +1\}^n$ on the resulting Ising model with n nodes is given by

$$p(\underline{\sigma}) = \frac{1}{Z} \exp \left(\sum_{(i,j) \in E} J_{ij}^* \sigma_i \sigma_j \right). \quad (\text{S1})$$

As noted earlier in Section 4.2, it is useful to view the initial spin configuration $\underline{\sigma}^0$ as a query to the Glauber dynamics which returns the output of $(\underline{\sigma}^1, I^1)$ in the M-regime, where I^1 is the identity of the spin being updated at time $t = 1$. The conditional probability of updating node i through Glauber dynamics in the M-regime is then given by

$$p(\sigma_i^1 | \underline{\sigma}^0, \delta_{i,I^1} = 1) = \frac{\exp \left[\sigma_i^1 \left(\sum_{j \in \partial i} J_{ij}^* \sigma_j^0 \right) \right]}{2 \cosh \left[\sum_{j \in \partial i} J_{ij}^* \sigma_j^0 \right]}. \quad (\text{S2})$$

where the initial probability distribution over $\underline{\sigma}^0$ is the uniform distribution over all possible spin configurations:

$$p(\underline{\sigma}^0 = \underline{\sigma}) = \frac{1}{2^n}, \quad \forall \underline{\sigma} \in \{-1, +1\}^n. \quad (\text{S3})$$

Using m samples $\{(\underline{\sigma}^{0(t)}, \underline{\sigma}^{1(t)}, I^{1(t)})\}_{t \in [m]}$ generated through Glauber dynamics (Eq. S2) in the M-regime, the Ising model is learned using the D-RISE and D-RPLE estimators which are based on the following (simplified) objectives:

$$\text{D-ISO: } \mathcal{S}_m(\underline{J}_u) = \frac{1}{m_u} \sum_{t=1}^m \exp \left[-\sigma_u^{1(t)} \left(\sum_{i \neq u} J_{ui} \sigma_i^{0(t)} \right) \right] \delta_{u,I^{1(t)}}. \quad (\text{S4})$$

$$\text{D-PL: } \mathcal{L}_i(\underline{J}_u) = -\frac{1}{m_u} \sum_{t=1}^m \ln \left[1 + \sigma_u^{1(t)} \tanh \left(\sum_{i \neq u} J_{ui} \sigma_i^{0(t)} \right) \right] \delta_{u,I^{1(t)}}. \quad (\text{S5})$$

The above objective functions are given for recovering the neighborhood around node u . The analysis of the D-RISE and D-RPLE estimators closely follows the work of (Vuffray et al., 2016) which analyzed the case of learning from i.i.d. samples. We are now in a position to state formal theorems regarding estimation error and sample complexity of structure learning of the estimators D-RISE and D-RPLE.

Theorem 2 (M-regime: Error Bound on Estimates). *Let $\{(\underline{\sigma}^t, \underline{\sigma}^{t+1}, I^{t+1})\}_{t=0, \dots, m-1}$ be m samples of spin configurations and corresponding node identities drawn through Glauber dynamics (Eq. 2), and define $m_i = \sum_{t=1}^m \delta_{i,I^{t+1}}$ as the number of updates per spin i . Considering M-regime on an Ising model with maximum degree d , maximum coupling intensity β , and assume $H_i^* = 0 \forall i$. Then for any $\delta > 0$, the square error of the following estimators with the following choices of penalty parameter $\lambda \propto \sqrt{\frac{\ln(3n^3/\delta)}{m_u}}$ is bounded with probability at least $1 - \delta$ for all nodes $u \in V$ if the number of samples satisfies*

i) *D-RPLE: If $m_u \geq 2^{17} d^2 \exp(4\beta d) \ln \frac{3n^3}{\delta}$ for $\lambda = 4\sqrt{2} \sqrt{\frac{\ln(3n^3/\delta)}{m_u}}$ then $\|\hat{\underline{J}}_u - \underline{J}_u^*\|_2 \leq 240\sqrt{2d} \exp(2\beta d) \sqrt{\frac{\ln \frac{3n^3}{\delta}}{m_u}}$,*

ii) *D-RISE: If $m_u \geq 2^{14} d^2 \exp(2\beta d) \ln \frac{3n^3}{\delta}$ for $\lambda = 4\sqrt{\frac{\ln(3n^3/\delta)}{m_u}}$ then $\|\hat{\underline{J}}_u - \underline{J}_u^*\|_2 \leq 240\sqrt{d} \exp(\beta d) \sqrt{\frac{\ln \frac{3n^3}{\delta}}{m_u}}$.*

The following theorem quantifies the sample complexity required for structure learning for the different estimators.

Theorem 3 (M-regime: Structure Learning of Ising Model Dynamics). *Let $\{(\underline{\sigma}^t, \underline{\sigma}^{t+1}, I^{t+1})\}_{t=0, \dots, m-1}$ be m samples of spin configurations and corresponding node identities drawn through Glauber dynamics (Eq. 2), and define $m_i = \sum_{t=1}^m \delta_{i, I^{t+1}}$ as the number of updates per spin i . Consider M-regime on an Ising model with maximum degree d , maximum coupling intensity β , minimum coupling intensity α , and assume $H_i^* = 0 \forall i$. Then for any $\delta > 0$, the following estimators with specified penalty parameter of form $\lambda \propto \sqrt{\frac{\ln(3n^3/\delta)}{m_u}}$ reconstructs the edge-set perfectly with probability $p(\hat{E}(\lambda, \alpha) = E) \geq 1 - \delta$ if the number of samples satisfies*

$$i) \text{ D-RPLE: } m_u \geq \max(d, \alpha^{-2}) 2^{19} d \exp(4\beta d) \ln \frac{3n^3}{\delta} \text{ for } \lambda = 4\sqrt{2} \sqrt{\frac{\ln(3n^3/\delta)}{m_u}},$$

$$ii) \text{ D-RISE: } m_u \geq \max(d, \alpha^{-2}) 2^{18} d \exp(2\beta d) \ln \frac{3n^3}{\delta} \text{ for } \lambda = 4\sqrt{\frac{\ln(3n^3/\delta)}{m_u}}.$$

Remark: Given the choice of the initial distribution $p(\underline{\sigma}_0)$ to be the uniform distribution, the total number of samples m required to get the number of samples m_u that satisfy Theorems 2 and 3 is $m = O(nm_u)$.

S1.1. Conditions for controlling estimation error

In order to control the error of the D-RISE and D-RPLE estimators, we enforce conditions shown to be sufficient in (Negahban et al., 2009) for such ℓ_1 -regularized M-estimators. These conditions are similar to the ones shown in (Vuffray et al., 2016) and are restated here for completeness. We state them considering the D-RISE estimator but they hold for the D-RPLE estimator as well.

Condition 1. *The ℓ_1 -penalty parameter strongly enforces regularization if it is greater than any partial derivatives of the objective function at $\underline{J}_u = \underline{J}_u^*$*

$$\|S_m(\underline{J}_u^*)\|_\infty \leq \frac{\lambda}{2}. \quad (\text{S6})$$

The above condition ensures that \underline{J}_u^* has at most d non-zero components and then the difference of the estimates $\Delta_u = \hat{J}_u - \underline{J}_u^*$ lies within the set

$$K := \left\{ \Delta_u \in \mathbb{R}^{n-1} \mid \|\Delta_u\|_1 \leq 4\sqrt{d} \|\Delta_u\|_2 \right\}. \quad (\text{S7})$$

Denoting the residual of the first order Taylor expansion of the objective function of the estimator:

$$\delta S_m(\Delta, \underline{J}_u^*) = S_m(\underline{J}_u^* + \Delta) - S_m(\underline{J}_u^*) - \langle \nabla S_m(\underline{J}_u^*), \Delta \rangle. \quad (\text{S8})$$

Condition 2. *The objective function is restricted strongly convex with respect to K on a ball of radius R centered at $\underline{J}_u = \underline{J}_u^*$, if for all $\Delta_u \in K$ such that $\|\Delta_u\|_2 \leq R$, there exists a constant $\kappa > 0$ such that*

$$\delta S_m(\Delta_u, \underline{J}_u^*) \geq \kappa \|\Delta_u\|_2^2. \quad (\text{S9})$$

The above condition ensures that the objective function is strongly convex in a restricted subset of \mathbb{R}^{n-1} . The following proposition shows that estimation error can be controlled if the above two conditions are satisfied.

Proposition 1 (Vuffray et al., 2016)). *If an ℓ_1 -regularized M-estimator satisfies Condition 1 and Condition 2 with $R > 3\sqrt{d}\frac{\lambda}{\kappa}$ then the error is bounded by*

$$\|\hat{J}_u - \underline{J}_u^*\|_2 \leq 3\sqrt{d} \frac{\lambda}{\kappa} \quad (\text{S10})$$

S1.2. Proof of the error bound estimation

For the presentation convenience, we first state Propositions that are useful for the proof. These proofs for these Propositions are given further below.

S1.2.1. D-RISE ESTIMATOR

Proposition 2 (Gradient concentration of D-RISE). *For some node $u \in V$, let $m_u \geq \exp(2\beta d) \ln \frac{2n}{\delta_1}$, then with probability at least $1 - \delta_1$, the components of the gradient of the D-ISO are bounded from above as*

$$\|S_m(\underline{J}_u^*)\|_\infty \leq \epsilon_1 \quad (\text{S11})$$

where $\epsilon_1 = 2\sqrt{\frac{\ln \frac{2n}{\delta_1}}{m_u}}$.

Proposition 3 (Restricted Strong Convexity for D-RISE). *For some node $u \in V$, let $m_u \geq 2^{11} d^2 \ln \frac{n^2}{\delta_2}$, then with probability at least $1 - \delta_2$, the residual of the first order Taylor expansion of D-ISO satisfies*

$$\delta S_m(\Delta_u, \underline{J}_u^*) \geq \exp(-\beta d) \frac{\|\Delta_u\|_2^2}{4(1 + 2\sqrt{d}R)}, \quad (\text{S12})$$

for all $\|\Delta_u\|_2 \leq R$.

Proof of Theorem 2(ii). Error bound on D-RISE: Let $\delta_1 = \frac{2\delta}{3n}$ and $\delta_2 = \frac{\delta}{3n}$ and $m_u \geq 2^{14} d^2 \exp(2\beta d) \ln \frac{3n^3}{\delta}$. Consider any node $u \in V$ and let \hat{J}_u be an optimal point of the D-ISO and $\Delta = \hat{J}_u - \underline{J}_u^*$. Using the values of λ and κ found in Proposition 2 and Proposition 3, we will look for values of R that satisfy

$$R > 3\sqrt{d} \frac{\lambda}{\kappa} = 12\sqrt{d}\lambda(1 + 2\sqrt{d}R) \exp(\beta d). \quad (\text{S13})$$

The above inequality is satisfied for $R = 2/\sqrt{d}$. Therefore, we can apply Proposition 1 for each node u and using the union bound, we find that the error is bounded in ℓ_2 -norm with probability at least $1 - \delta$ for all nodes by the following quantity,

$$\left\| \hat{J}_u - \underline{J}_u^* \right\|_2 \leq 240\sqrt{d} \exp(\beta d) \sqrt{\frac{\ln \frac{3n^3}{\delta}}{m_u}}. \quad (\text{S14})$$

□

S1.2.2. D-RPLE ESTIMATOR

Proposition 4 (Gradient concentration of D-RPLE). *For some node $u \in V$, let $m_u \geq \exp(2\beta d) \ln \frac{2n}{\delta_1}$, then with probability at least $1 - \delta_1$, the components of the gradient of the D-PL are bounded from above as*

$$\|\mathcal{L}_m(\underline{J}_u^*)\|_\infty \leq \epsilon_1 \quad (\text{S15})$$

where $\epsilon_1 = 2\sqrt{2}\sqrt{\frac{\ln \frac{2n}{\delta_1}}{m_u}}$.

Proposition 5 (Restricted Strong Convexity for D-RPLE). *For some node $u \in V$, let $m_u \geq 2^{11} d^2 \ln \frac{n^2}{\delta_2}$, then with probability at least $1 - \delta_2$, the residual of the first order Taylor expansion of D-PL satisfies*

$$\delta \mathcal{L}_m(\Delta_u, \underline{J}_u^*) \geq \exp(-2\beta d) \frac{\|\Delta_u\|_2^2}{4(1 + 4\sqrt{d}R)} \quad (\text{S16})$$

Proof of Theorem 2(i). Error bound on D-RPLE: Let $\delta_1 = \frac{2\delta}{3n}$ and $\delta_2 = \frac{\delta}{3n}$ and $m_u \geq 2^{17} d^2 \exp(4\beta d) \ln \frac{3n^3}{\delta}$. Consider any node $u \in V$ and let \hat{J}_u be an optimal point of the D-PL and $\Delta = \hat{J}_u - \underline{J}_u^*$. Using the values of λ and κ found in Proposition 4 and Proposition 5, we will look for values of R that satisfy

$$R > 3\sqrt{d} \frac{\lambda}{\kappa} = 12\sqrt{d}\lambda(1 + 4\sqrt{d}R) \exp(2\beta d). \quad (\text{S17})$$

The above inequality is satisfied for $R = 1/\sqrt{d}$. Therefore, we can apply Proposition 1 and find that the error is bounded in ℓ_2 -norm by the following quantity,

$$\left\| \hat{J}_u - J_u^* \right\|_2 \leq 240\sqrt{2}\sqrt{d} \exp(2\beta d) \sqrt{\frac{\ln \frac{3n^3}{\delta}}{m_u}}. \quad (\text{S18})$$

The theorem follows by application of the union bound over all nodes. \square

S1.3. Proof of structure learning theorem

Proof of Theorem 3. It is a simple application of Theorem 2 for an error equal to $\alpha/2$. \square

S1.4. Gradient Concentration

S1.4.1. D-RISE ESTIMATOR

Gradient of D-ISO (Eq. S4) is given by:

$$\frac{\partial}{\partial J_{uk}} S_m(J_u) = \frac{1}{m_u} \sum_{t=1}^m -\sigma_u^{1(t)} \sigma_k^{0(t)} \exp \left[- \sum_{i \in V \setminus u} J_{ui} \sigma_u^{1(t)} \sigma_i^{0(t)} \right] \delta_{u, I^1(t)} \quad (\text{S19})$$

where $m_u = \sum_{t=1}^m \delta_{u, I^1(t)}$. Let us denote the term in the above summation as the following random variable

$$X_{uk}(J_u) = -\sigma_u^1 \sigma_k^0 \exp \left[- \sum_{i \in V \setminus u} J_{ui} \sigma_u^1 \sigma_i^0 \right] \quad \forall k \in \partial u \quad (\text{S20})$$

The lemma below indicates that the D-RISE estimator is consistent and unbiased regardless of the choice of $p(\underline{\sigma}^0)$. This will also be useful for the concentration inequality to come after.

Lemma 1. For any $u \in V$ and $k \in V \setminus u$, we have

$$\mathbb{E}[X_{uk}(J_u^*)] = 0 \quad (\text{S21})$$

Proof of Lemma 1. Let us note the probability distribution with respect to which we take the expectation.

$$\mathbb{E}_{p(\sigma_u^1, \underline{\sigma}^0 | \delta_{u, I^1} = 1)} [X_{uk}(J_u^*)] \quad (\text{S22})$$

$$= \mathbb{E}_{p(\sigma_u^1 | \underline{\sigma}^0, \delta_{u, I^1} = 1) p(\underline{\sigma}^0)} [X_{uk}(J_u^*)] \quad (\text{S23})$$

$$= \sum_{\underline{\sigma}^0} \left[\sum_{\sigma_u^1} p(\sigma_u^1 | \underline{\sigma}^0, \delta_{u, I^1} = 1) p(\underline{\sigma}^0) X_{uk}(J_u^*) \right] \quad (\text{S24})$$

$$= \sum_{\underline{\sigma}^0} p(\underline{\sigma}^0) \left[\sum_{\sigma_u^1} p(\sigma_u^1 | \underline{\sigma}^0, \delta_{u, I^1} = 1) X_{uk}(J_u^*) \right] \quad (\text{S25})$$

$$= \sum_{\underline{\sigma}^0} \frac{p(\underline{\sigma}^0)}{2 \cosh \left(\sum_{j \in \partial u} J_{uj}^* \sigma_j^0 \right)} \left[\sum_{\sigma_u^1} -\sigma_u^1 \sigma_k^0 \exp \left(\sigma_u^1 \left(\sum_{j \in \partial u} J_{uj}^* \sigma_j^0 - \sum_{l \in \partial u} J_{ul}^* \sigma_l^0 \right) \right) \right] \quad (\text{S26})$$

$$= 0 \quad (\text{S27})$$

where in the first step, we used the law of total expectations. In the second to last step, we used the definition of X_{uk} from Eq. S20 and the conditional probability from Eq. S2. \square

Lemma 2. For any Ising model with n spins considering $u \in V$ and $k \in V \setminus u$, we have

$$\mathbb{E}[X_{uk}(\underline{J}_u^*)^2] = 1 \quad (\text{S28})$$

Proof of Lemma 2. From direct computation, we have

$$\mathbb{E}_{p(\sigma_u^1, \underline{\sigma}^0 | \delta_{u,I^1}=1)}[X_{uk}(\underline{J}_u^*)^2] \quad (\text{S29})$$

$$= \sum_{\underline{\sigma}^0} p(\underline{\sigma}^0) \left[\sum_{\sigma_u^1} p(\sigma_u^1 | \underline{\sigma}^0, \delta_{u,I^1} = 1) X_{uk}(\underline{J}_u^*)^2 \right] \quad (\text{S30})$$

$$= \sum_{\underline{\sigma}^0} \frac{p(\underline{\sigma}^0)}{2 \cosh \left(\sum_{j \in \partial u} J_{uj}^* \sigma_j^0 \right)} \left[\sum_{\sigma_u^1} \exp \left(-\sigma_u^1 \sum_{j \in \partial u} J_{uj}^* \sigma_j^0 \right) \right] \quad (\text{S31})$$

$$= \sum_{\underline{\sigma}^0} p(\underline{\sigma}^0) \quad (\text{S32})$$

$$= 1 \quad (\text{S33})$$

where in the second step we noted that $(\sigma_i^1)^2 = (\sigma_i^0)^2 = 1$ when substituting for X_{uk} from Eq. S20. \square

Lemma 3. For any Ising model with n spins with maximum degree d and maximum interaction strength β , we have for $k \neq u \in V$, we have

$$|X_{uk}(\underline{J}_u^*)| \leq \exp(\beta d) \quad (\text{S34})$$

Proof of Lemma 3.

$$|X_{uk}(\underline{J}_u^*)| = \left| -\sigma_u^1 \sigma_k^0 \exp \left(- \sum_{i \in \partial u} J_{ui}^* \sigma_u^1 \sigma_i^0 \right) \right| \quad (\text{S35})$$

$$= \exp \left(- \sum_{i \in \partial u} J_{ui}^* \sigma_u^1 \sigma_i^0 \right) \quad (\text{S36})$$

$$\leq \exp(\beta d) \quad (\text{S37})$$

where we firstly noted that $\delta_{u,I^1} \in \{0, 1\}$. In the second step, we noted that the components of \underline{J}_u^* have a maximum value of β and at most d of them are non-zero. Further $|\sigma_u^1 \sigma_i^0| = 1$ as spins take values in $\{-1, +1\}$. \square

In the M-regime, the different tuples of realizations of $(\underline{\sigma}^1, \underline{\sigma}^0, I^1)$ are independent of each other. This allows us to use the lemmas obtained above and obtain a concentration inequality in the following proof.

Proof of Proposition 2. Utilizing Lemmas 1, 2 and 3 combined with Bernstein's inequality, we have

$$p \left[\left| \frac{\partial}{\partial J_{uk}} S_m(\underline{J}_u^*) \right| > a \right] \leq 2 \exp \left(- \frac{\frac{1}{2} a^2 m_u}{1 + \frac{1}{3} \exp(\beta d) a} \right) \quad (\text{S38})$$

Setting

$$s = \frac{\frac{1}{2} a^2 m_u}{1 + \frac{1}{3} \exp(\beta d) a}, \quad (\text{S39})$$

and considering $z = \frac{s}{m_u} \exp(\beta d)$, we can write

$$p \left[\left| \frac{\partial}{\partial J_{uk}} S_m(\underline{J}_u^*) \right| > \frac{1}{3} \left(z + \sqrt{\frac{18z}{\exp(\beta d)} + z^2} \right) \right] \leq 2 \exp(-s) \quad (\text{S40})$$

For $m_u \geq s \exp(2\beta d)$, we have $z^2 = \frac{s^2}{m_u^2} \exp(2\beta d) \leq \frac{s}{m_u}$ and that

$$\frac{1}{3} \left(z + \sqrt{\frac{18z}{\exp(-\beta d)} + z^2} \right) \leq \frac{1}{3} \left(\sqrt{\frac{s}{m_u}} + \sqrt{\frac{18s}{m_u} + \frac{s}{m_u}} \right) \quad (\text{S41})$$

$$\leq \frac{\sqrt{19} + 1}{3} \sqrt{\frac{s}{m_u}} \quad (\text{S42})$$

$$\leq 2 \sqrt{\frac{s}{m_u}} \quad (\text{S43})$$

which allows us to simplify Eq. S40:

$$p \left[\left| \frac{\partial}{\partial J_{uk}} S_m(\underline{J}_u^*) \right| > 2 \sqrt{\frac{s}{m_u}} \right] \leq 2 \exp(-s) \quad (\text{S44})$$

Setting $s = \ln \frac{2n}{\delta_1}$ and taking the union bound over every component of the gradient gives us the desired result. \square

S1.4.2. D-RPLE ESTIMATOR

Gradient of D-PL (Eq. S45) is given by:

$$\frac{\partial}{\partial J_{uk}} = \frac{1}{m_u} \sum_{t=1}^m \sigma_k^{0(t)} \left[\tanh \left(\sum_{i \neq u} J_{ui} \sigma_i^{0(t)} \right) - \sigma_u^{1(t)} \right] \delta_{u, I^1(t)}. \quad (\text{S45})$$

Let us denote the term in the above summation as the following random variable

$$Z_{uk}(\underline{J}_u) = \sigma_k^{0(t)} \left[\tanh \left(\sum_{i \neq u} J_{ui} \sigma_i^{0(t)} \right) - \sigma_u^{1(t)} \right] \quad \forall k \in \partial u \quad (\text{S46})$$

The lemma below indicates that the D-RPLE estimator is consistent and unbiased regardless of the choice of $p(\underline{\sigma}^0)$. This will also be useful for the concentration inequality to come after.

Lemma 4. *For any $u \in V$ and $k \in V \setminus u$, we have*

$$\mathbb{E}[Z_{uk}(\underline{J}_u^*)] = 0 \quad (\text{S47})$$

Proof of Lemma 4. Let us note the probability distribution with respect to which we take the expectation.

$$\mathbb{E}_{p(\sigma_u^1, \underline{\sigma}^0 | \delta_{u, I^1} = 1)}[Z_{uk}(\underline{J}_u^*)] \quad (\text{S48})$$

$$= \sum_{\underline{\sigma}^0} \left[\sum_{\sigma_u^1} p(\sigma_u^1 | \underline{\sigma}^0, \delta_{u, I^1} = 1) p(\underline{\sigma}^0) Z_{uk}(\underline{J}_u^*) \right] \quad (\text{S49})$$

$$= \sum_{\underline{\sigma}^0} p(\underline{\sigma}^0) \left[\sum_{\sigma_u^1} p(\sigma_u^1 | \underline{\sigma}^0, \delta_{u, I^1} = 1) Z_{uk}(\underline{J}_u^*) \right] \quad (\text{S50})$$

$$= \sum_{\underline{\sigma}^0} p(\underline{\sigma}^0) \left[\sum_{\sigma_u^1} \frac{\exp \left[\sigma_u^1 (\sum_{j \in \partial u} J_{uj}^* \sigma_j^0) \right]}{2 \cosh \left[\sum_{j \in \partial u} J_{uj}^* \sigma_j^0 \right]} \sigma_k^{0(t)} \left(\tanh \left(\sum_{i \neq u} J_{ui} \sigma_i^{0(t)} \right) - \sigma_u^{1(t)} \right) \right] \quad (\text{S51})$$

$$= \sum_{\underline{\sigma}^0} p(\underline{\sigma}^0) \sigma_k^{0(t)} \left[\tanh \left(\sum_{i \neq u} J_{ui} \sigma_i^{0(t)} \right) - \sum_{\sigma_u^1} \frac{\exp \left[\sigma_u^1 (\sum_{j \in \partial u} J_{uj}^* \sigma_j^0) \right]}{2 \cosh \left[\sum_{j \in \partial u} J_{uj}^* \sigma_j^0 \right]} \sigma_u^{1(t)} \right] \quad (\text{S52})$$

$$= \sum_{\underline{\sigma}^0} p(\underline{\sigma}^0) \sigma_k^{0(t)} \left[\tanh \left(\sum_{i \neq u} J_{ui} \sigma_i^{0(t)} \right) - \tanh \left(\sum_{i \neq u} J_{ui} \sigma_i^{0(t)} \right) \right] \quad (\text{S53})$$

$$= 0 \quad (\text{S54})$$

where in the first step, we used the law of total expectations. In the third to last step, we used the definition of Z_{uk} from Eq. S46 and the conditional probability from Eq. S2. \square

Lemma 5. *For any Ising model with n spins with maximum degree d and maximum interaction strength β , we have for $k \neq u \in V$, we have*

$$|Z_{uk}(\underline{J}_u^*)| \leq 2 \quad (\text{S55})$$

Proof of Lemma 5.

$$|Z_{uk}(\underline{J}_u^*)| = \left| \sigma_k^{0(t)} \left[\tanh \left(\sum_{i \neq u} J_{ui} \sigma_i^{0(t)} \right) - \sigma_u^{1(t)} \right] \right| \quad (\text{S56})$$

$$\leq \left| \tanh \left(\sum_{i \neq u} J_{ui} \sigma_i^{0(t)} \right) \right| + \left| \sigma_u^{1(t)} \right| \quad (\text{S57})$$

$$\leq 2 \quad (\text{S58})$$

where in the last step, we noted that $|\tanh(\cdot)| \leq 1$ and $|\sigma_u^1| = 1$ as spins take values in $\{-1, +1\}$. \square

As noted before, the different tuples of realizations of $(\underline{\sigma}^1, \underline{\sigma}^0, I^1)$ are independent of each other in the M-regime. We use the lemmas obtained above and obtain a concentration inequality in the following proof.

Proof of Proposition 4. Utilizing Lemmas 4 and 5 combined with Hoeffding's inequality, we have

$$p \left[\left| \frac{\partial}{\partial J_{uk}} \mathcal{L}_m(\underline{J}_u^*) \right| > a \right] \leq 2 \exp \left(-\frac{m_u a^2}{8} \right) \quad (\text{S59})$$

Let $a = 2\sqrt{2} \sqrt{\frac{s}{m_u}}$. We then have

$$p \left[\left| \frac{\partial}{\partial J_{uk}} \mathcal{L}_m(\underline{J}_u^*) \right| > 2\sqrt{2} \sqrt{\frac{s}{m_u}} \right] \leq 2 \exp(-s) \quad (\text{S60})$$

Setting $s = \ln \frac{2n}{\delta_1}$ and taking the union bound over every component of the gradient gives us the desired result. \square

S1.5. Restricted Strong Convexity

The following deterministic functional inequality derived in (Vuffray et al., 2016) will be useful for latter results.

Lemma 6. *The following inequality holds for all $z \in \mathbb{R}$.*

$$e^{-z} - 1 + z \geq \frac{z^2}{2 + |z|}. \quad (\text{S61})$$

We will also find the following deterministic functional inequality useful.

Lemma 7. *The following inequality holds for all $z \in \mathbb{R}$ and for any $x \in \mathbb{R}$.*

$$-\ln(1 + \tanh(x + z)) + \ln(1 + x) + z(1 - \tanh(x)) \geq \frac{z^2}{2(1 + |z|)} \operatorname{sech}^2(x). \quad (\text{S62})$$

Proof of Lemma 7. Let us denote the function

$$f(x, z) := -\ln(1 + \tanh(x + z)) + \ln(1 + x) + z(1 - \tanh(x)) \quad (\text{S63})$$

and the auxillary function

$$g(x, z) := 2(1 + |z|)f(x, z) - \operatorname{sech}^2(x)z^2. \quad (\text{S64})$$

We show that for fixed $x \in \mathbb{R}$ and $z = 0$, $g(x, z)$ achieves its minimum at $g(x, 0) = 0$. Observe the first partial derivative of $g(x, z)$ wrt z is given by

$$\frac{\partial}{\partial z} g(x, z) = \begin{cases} 2f(x, z) + 2(1+z)(\tanh(x+z) - \tanh(x)) - 2z \operatorname{sech}^2(x), & z > 0 \\ -2f(x, z) + 2(1-z)(\tanh(x+z) - \tanh(x)) - 2z \operatorname{sech}^2(x), & z < 0 \end{cases} \quad (\text{S65})$$

We note that the partial derivatives vanishes at zero from both the negative and positive directions of z :

$$\lim_{z \rightarrow 0^+} \frac{\partial}{\partial z} g(x, z) = \lim_{z \rightarrow 0^-} \frac{\partial}{\partial z} g(x, z) = 0 \quad (\text{S66})$$

The second partial derivatives of $g(x, z)$ are given by

$$\frac{\partial^2}{\partial z^2} g(x, z) = \begin{cases} 4(\tanh(x+z) - \tanh(x)) + 2(1+z) \operatorname{sech}^2(x+z) - 2 \operatorname{sech}^2(x), & z > 0 \\ 4(\tanh(x) - \tanh(x-z)) + 2(1-z) \operatorname{sech}^2(x+z) - 2 \operatorname{sech}^2(x), & z < 0 \end{cases} \quad (\text{S67})$$

We note that for $z > 0$, $\frac{\partial^2}{\partial z^2} g(x, z)$ is non-negative

$$\frac{\partial^2}{\partial z^2} g(x, z) = 4(\tanh(x+z) - \tanh(x)) + 2(1+z) \operatorname{sech}^2(x+z) - 2 \operatorname{sech}^2(x) \quad (\text{S68})$$

$$> 4(\tanh(x+z) - \tanh(x)) + 2 \operatorname{sech}^2(x+z) - 2 \operatorname{sech}^2(x) \quad (\text{S69})$$

$$= 4(\tanh(x+z) - \tanh(x)) + 2(\tanh^2(x) - 2 \tanh^2(x+z)) \quad (\text{S70})$$

$$= 2(\tanh(x+z) - \tanh(x))(2 - \tanh(x) - \tanh(x+z)) \quad (\text{S71})$$

$$> 0 \quad (\text{S72})$$

where in the last step, we noted that $\tanh(x)$ is a monotonically increasing function and that $\tanh(x) < 1$. A similar result can be shown for $z < 0$. Combining this with Eq. S66, we prove that for all z and any x , $g(x, z) \geq g(x, 0) = 0$ which gives us our desired result. \square

Let H_{ij} denote the correlation matrix elements

$$H_{ij} = \mathbb{E}_{p(\sigma_u^1, \underline{\sigma}^0 | \delta_{u, I^1} = 1)} [\sigma_i^0 \sigma_j^0] \quad (\text{S73})$$

and we denote the corresponding matrix as $H = [H_{ij}] \in \mathbb{R}^{|\partial u| \times |\partial u|}$. Let the empirical estimate of the correlation matrix be denoted by \hat{H} and the matrix elements be given by

$$\hat{H}_{ij} = \frac{1}{m_u} \sum_{t=1}^m \sigma_i^{0(t)} \sigma_j^{0(t)} \delta_{u, I^{1(t)}} \quad (\text{S74})$$

Lemma 8. Consider some node $u \in V$. With probability at least $1 - n^2 \exp\left(-\frac{m_u \epsilon_2^2}{2}\right)$, we have

$$|\hat{H}_{ij} - H_{ij}| \leq \epsilon_2 \quad (\text{S75})$$

for all $i, j \in \partial u$ and $\epsilon_2 > 0$.

Proof of Lemma 8. Fix $i, j \in \partial u$. Noting that $|\sigma_i^0 \sigma_j^0 \delta_{u, I^1}| \leq 1$ and combining with Hoeffding's inequality:

$$p(|\hat{H}_{ij} - H_{ij}| > \epsilon_2) \leq 2 \exp\left(-\frac{m_u \epsilon_2^2}{2}\right) \quad (\text{S76})$$

The proof follows by noting that the matrix H is symmetric allowing us to take the union bound over all $i < j \in V \setminus u$. \square

Lemma 9. Consider an Ising model with n spins and some node $u \in V$, then the following holds for the Hessian

$$\Delta_u^T H \Delta_u = \|\Delta_u\|_2^2 \quad (\text{S77})$$

Proof of Lemma 9. From direct evaluation of H , we have

$$H_{ij} = \mathbb{E}[\sigma_i^0 \sigma_j^0] \quad (\text{S78})$$

$$= \sum_{\underline{\sigma}^0} p(\underline{\sigma}^0) \sum_{\sigma_u^1} p(\sigma_u^1 | \underline{\sigma}^0, \delta_{u, I^1} = 1) \sigma_i^0 \sigma_j^0 \quad (\text{S79})$$

$$= \sum_{\underline{\sigma}^0} p(\underline{\sigma}^0) \sigma_i^0 \sigma_j^0 \quad (\text{S80})$$

$$= \delta_{ij} \quad (\text{S81})$$

where $\delta_{ij} = 1$ iff $i = j$. Thus the correlation matrix $H = I$ where I is an identity matrix of size $\mathbb{R}^{|\partial u| \times |\partial u|}$. We assumed that the initial distribution of $p(\underline{\sigma}^0)$ is given by Eq. S3. The proof follows from computation of $\Delta_u^T H \Delta_u$. \square

S1.5.1. D-RISE ESTIMATOR

Lemma 10. *The residual of the first order Taylor expansion of the D-ISO satisfies*

$$\delta S_m(\Delta_u, \underline{J}_u^*) \geq \exp(-\beta d) \frac{\Delta_u^T \hat{H} \Delta_u}{2 + \|\Delta_u\|_1}. \quad (\text{S82})$$

Proof of Lemma 10. Noting the expression of the residual from Eq. S8 and that $\langle \nabla S_m(\underline{J}_u^*), \Delta_u \rangle = \sum_{k \in \partial u} \left[\frac{\partial}{\partial J_{uk}} S_m(\underline{J}_u^*) \right] \Delta_{uk}$, we have that

$$\begin{aligned} \delta S_m(\Delta_u, \underline{J}_u^*) &= \frac{1}{m_u} \sum_{t=1}^m \exp \left(- \sum_{k \in \partial u} J_{uk}^* \sigma_u^{1(t)} \sigma_k^{0(t)} \right) \delta_{u, I^{1(t)}} \times \\ &\quad \left[\exp \left(- \sum_{k \in \partial u} \Delta_{uk} \sigma_u^{1(t)} \sigma_k^{0(t)} \right) - 1 + \sum_{k \in \partial u} \Delta_{uk} \sigma_u^{1(t)} \sigma_k^{0(t)} \right] \end{aligned} \quad (\text{S83})$$

$$\geq \exp(-\beta d) \frac{\Delta_u^T \hat{H} \Delta_u}{2 + \left| \sum_{k \in \partial u} \Delta_{uk} \sigma_u^{1(t)} \sigma_k^{0(t)} \right|}. \quad (\text{S84})$$

where in the second step we used Lemma 6. The proof follows by observing that $|\sum_{k \in \partial u} \Delta_{uk} \sigma_u^{1(t)} \sigma_k^{0(t)}| \leq \|\Delta_u\|_1$. \square

Proof of Proposition 3. Using Lemma 10 and for $m_u \geq \frac{2}{\epsilon_2^2} \ln \frac{n^2}{\delta_2}$, the residual satisfies the following with probability at least $1 - \delta_2$:

$$\delta S_m(\Delta_u, \underline{J}_u^*) \geq \exp(-\beta d) \frac{\Delta_u^T \hat{H} \Delta_u}{2 + \|\Delta_u\|_1} \quad (\text{S85})$$

$$= \exp(-\beta d) \frac{\Delta_u^T H \Delta_u + \Delta_u^T (H - \hat{H}) \Delta_u}{2 + \|\Delta_u\|_1} \quad (\text{S86})$$

$$\stackrel{(a)}{\geq} \exp(-\beta d) \frac{\Delta_u^T H \Delta_u - \epsilon_2 \|\Delta_u\|_u^2}{2 + \|\Delta_u\|_1} \quad (\text{S87})$$

$$\stackrel{(b)}{\geq} \exp(-\beta d) \frac{\|\Delta_u\|_2^2 - \epsilon_2 \|\Delta_u\|_1^2}{2 + \|\Delta_u\|_1} \quad (\text{S88})$$

where we used Lemma 8 in (a) and Lemma 9 in (b). Setting $\epsilon_2 = \frac{1}{32d}$, we note that

$$-\epsilon_2 \|\Delta_u\|_1^2 \geq -\frac{1}{2} \|\Delta_u\|_2^2 \quad (\text{S89})$$

where we have used Condition S9 that $\|\Delta_u\|_1 \leq 4\sqrt{d} \|\Delta_u\|_2$. Combining this with $\|\Delta_u\|_2 \leq R$, we obtain the desired result. \square

S1.5.2. D-RPLE ESTIMATOR

Consider the first order Taylor expansion:

$$\delta\mathcal{L}_m(\Delta, \underline{J}_u^*) = \mathcal{L}_m(\underline{J}_u^* + \Delta) - \mathcal{L}_m(\underline{J}_u^*) - \langle \nabla \mathcal{L}_m(\underline{J}_u^*), \Delta \rangle. \quad (\text{S90})$$

Lemma 11. *The residual of the first order Taylor expansion of the D-PL satisfies*

$$\delta\mathcal{L}_m(\Delta_u, \underline{J}_u^*) \geq \exp(-2\beta d) \frac{\Delta_u^T \hat{H} \Delta_u}{2(1 + \|\Delta_u\|_1)}. \quad (\text{S91})$$

Proof of Lemma 11. Noting the expression of the residual from Eq. S90 and that $\langle \nabla \mathcal{L}_m(\underline{J}_u^*), \Delta_u \rangle = \sum_{k \in \partial u} \left[\frac{\partial}{\partial J_{uk}} \mathcal{L}_m(\underline{J}_u^*) \right] \Delta_{uk}$, we have that

$$\begin{aligned} \delta\mathcal{L}_m(\Delta_u, \underline{J}_u^*) &= \frac{1}{m_u} \sum_{t=1}^m - \left[\ln \left[1 + \sigma_u^{1(t)} \tanh \left(\sum_{i \neq u} (J_{ui} + \Delta_{ui}) \sigma_i^{0(t)} \right) \right] + \right. \\ &\quad \left. \ln \left[1 + \sigma_u^{1(t)} \tanh \left(\sum_{i \neq u} J_{ui} \sigma_i^{0(t)} \right) \right] + \sum_{k \in \partial u} \Delta_{uk} \sigma_k^{(0)} \sigma_u^{1(t)} \left[1 - \sigma_u^{1(t)} \tanh \left(\sum_{i \neq u} J_{ui} \sigma_i^{0(t)} \right) \right] \right] \end{aligned} \quad (\text{S92})$$

$$\begin{aligned} &\geq \frac{1}{m_u} \sum_{t=1}^m \frac{\left(\sum_{k \in \partial u} \Delta_{uk} \sigma_u^{1(t)} \sigma_k^{0(t)} \right)^2}{2 \left(1 + \left| \sum_{k \in \partial u} \Delta_{uk} \sigma_u^{1(t)} \sigma_k^{0(t)} \right| \right)} \operatorname{sech}^2 \left(\sum_{i \neq u} J_{ui} \sigma_i^{0(t)} \sigma_u^{1(t)} \right) \end{aligned} \quad (\text{S93})$$

$$\begin{aligned} &\geq \exp(-2\beta d) \frac{1}{m_u} \sum_{t=1}^m \frac{\left(\sum_{k \in \partial u} \Delta_{uk} \sigma_u^{1(t)} \sigma_k^{0(t)} \right)^2}{2 \left(1 + \left| \sum_{k \in \partial u} \Delta_{uk} \sigma_u^{1(t)} \sigma_k^{0(t)} \right| \right)} \end{aligned} \quad (\text{S94})$$

$$\geq \exp(-2\beta d) \frac{\Delta_u^T \hat{H} \Delta_u}{2(1 + \|\Delta_u\|_1)} \quad (\text{S95})$$

where in the second step, we used Lemma 7 combined with the fact that $\sigma_i \tanh(x) = \tanh(\sigma_i x)$ as $\sigma_i \in \{-1, +1\}$. In the third step, we noted that $\operatorname{sech}^2(x) = 1 - \tanh^2(x) \geq \exp(-2|x|)$ and $|\sum_{i \in \partial u} J_{ui} \sigma_i^{0(t)} \sigma_u^{1(t)}| \leq \beta d$. In the final step, we used the definition of \hat{H} and that $|\sum_{k \in \partial u} \Delta_{uk} \sigma_u^{1(t)} \sigma_k^{0(t)}| \leq \|\Delta_u\|_1$ to complete the proof. \square

Proof of Proposition 5. Using Lemma 11 and for $m_u \geq \frac{2}{\epsilon_2^2} \ln \frac{n^2}{\delta_2}$, the residual satisfies the following with probability at least $1 - \delta_2$:

$$\delta\mathcal{L}_m(\Delta_u, \underline{J}_u^*) \geq \exp(-2\beta d) \frac{\Delta_u^T \hat{H} \Delta_u}{2(1 + \|\Delta_u\|_1)} \quad (\text{S96})$$

$$= \exp(-2\beta d) k_1 \frac{\Delta_u^T H \Delta_u + \Delta_u^T (H - \hat{H}) \Delta_u}{2(1 + \|\Delta_u\|_1)} \quad (\text{S97})$$

$$\stackrel{(a)}{\geq} \exp(-2\beta d) \frac{\Delta_u^T H \Delta_u - \epsilon_2 \|\Delta_1\|_u^2}{2(1 + \|\Delta_u\|_1)} \quad (\text{S98})$$

$$\stackrel{(b)}{\geq} \exp(-2\beta d) \frac{\|\Delta_u\|_2^2 - \epsilon_2 \|\Delta_u\|_1^2}{2(1 + \|\Delta_u\|_1)} \quad (\text{S99})$$

where we used Lemma 8 in (a) and Lemma 9 in (b). Setting $\epsilon_2 = \frac{1}{32d}$, we note that

$$-\epsilon_2 \|\Delta_u\|_1^2 \geq -\frac{1}{2} \|\Delta_u\|_2^2 \quad (\text{S100})$$

where we have used Condition S9 that $\|\Delta_u\|_1 \leq 4\sqrt{d}\|\Delta_u\|_2$. Combining this with $\|\Delta_u\|_2 \leq R$, we obtain the desired result. \square

S2. Setup for numerical experiments

In this section, we describe the optimization techniques that we used in the implementation of D-RISE/D-RPLE estimators and the computer infrastructure that was used for running our numerical experiments.

S2.1. Optimization tools

The D-RISE and D-RPLE estimators involve optimization of a convex objective function. There are a variety of optimization techniques that can be used for this purpose including gradient descent type methods and interior point methods. For our numerical experiments, we used the interior point Ipopt (Biegler & Zavala, 2009) optimization package within the JuMP modeling framework for mathematical optimization in Julia.

As an alternative to the Ipopt software for optimization, we also implemented the coordinate descent (CD) method for D-RISE and D-RPLE as a part of our package. The idea is to perform gradient descent only along one coordinate at a time, and then cycle through coordinates until convergence. For example, the optimization problem for each node u in D-RISE is:

$$(\hat{J}_u, \hat{H}_u) = \underset{(J_u, H_u)}{\operatorname{argmin}} \left[\frac{1}{m_u} \sum_{t=1}^m \exp \left(-\sigma_u^{t+1} \left(\sum_{i \neq u} J_{ui} \sigma_i^t + H_u \right) \right) \delta_{u, I^{t+1}} + \lambda \|J_u\|_1 \right], \quad (\text{S101})$$

In coordinate descent, we optimize over one variable only at a time, e.g. over J_{uk} for some k . Once the minimum is found, we cycle through other components, and repeat until we reach the global minimum of the entire convex function. Interestingly, each iteration step is a solution of a one-dimensional optimization problem:

$$\hat{x} = \underset{x}{\operatorname{argmin}} \cosh x - \kappa \sinh x + \mu |x|, \quad (\text{S102})$$

where the constant κ and the regularization parameter μ is given by

$$\kappa = \frac{b}{a}, \quad \mu = \begin{cases} 0, & x = H_u \\ \lambda/a, & \text{otherwise.} \end{cases} \quad (\text{S103})$$

with

$$a = \begin{cases} \frac{1}{m_u} \sum_{t=1}^m \exp \left(-\sigma_u^{t+1} \sum_{i \neq u} J_{ui} \sigma_i^t \right) \delta_{u, I^{t+1}}, & x = H_u \\ \frac{1}{m_u} \sum_{t=1}^m \exp \left(-\sigma_u^{t+1} \left(\sum_{i \neq u, k} J_{ui} \sigma_i^t + H_u \right) \right) \delta_{u, I^{t+1}}, & x = J_{uk} \forall k \end{cases} \quad (\text{S104})$$

$$b = \begin{cases} \frac{1}{m_u} \sum_{t=1}^m \sigma_u^{t+1} \exp \left(-\sigma_u^{t+1} \sum_{i \neq u} J_{ui} \sigma_i^t \right) \delta_{u, I^{t+1}}, & x = H_u \\ \frac{1}{m_u} \sum_{t=1}^m \sigma_u^{t+1} \sigma_k^t \exp \left(-\sigma_u^{t+1} \left(\sum_{i \neq u, k} J_{ui} \sigma_i^t + H_u \right) \right) \delta_{u, I^{t+1}}, & x = J_{uk} \forall k \end{cases} \quad (\text{S105})$$

and the minimum can be found explicitly (after soft-thresholding):

$$\hat{x} = \begin{cases} \log \left(\frac{\sqrt{1-\kappa^2} + \mu^2 - \mu \operatorname{sign}(\kappa)}{1-\kappa} \right), & \mu < |\kappa| \\ 0, & \text{otherwise.} \end{cases} \quad (\text{S106})$$

Note that there is a slight difference in the optimization problem and solution depending on if the coordinate randomly chosen is a coupling parameter J_{ui} or magnetic field H_u . As a result of having access to the above analytical solution, coordinate descent for D-RISE does not require the choice of the step in the gradient descent. This simplification however does not occur for D-RPLE. At each step of the descent, the updated coordinate is chosen at random.

Another popular optimization method that may be applied to D-RISE and D-RPLE is stochastic gradient descent (SGD) method, although SGD requires tuning hyper-parameters such as learning rate and batch size of samples.

We note that other possible choices of optimization techniques include the entropic gradient descent method (Beck & Teboulle, 2003) (see (Vuffray et al., 2019) for a description of this method used in estimator RISE for the case of i.i.d. samples) and mirror gradient descent method of (Ben-Tal et al., 2001).

S2.2. Computational resources

The numerical experiments were run on a cluster. Each node of the cluster has a Intel Xeon Gold 6248 processor with 2×20 cores with 32GB RAM. We were able to take advantage of multiple cores on each node since learning local neighborhoods of each node in our algorithm is done independently and hence can be carried out in parallel. Jobs for different graphical model instances were distributed on the cluster. Parallelization is implemented in our package and example scripts for distributing jobs are included for completeness.

S3. Empirical selection of the regularization parameter c_λ

In this section, we describe the procedure that we used for selecting the values of the coefficient of the regularization parameter c_λ for the estimators of D-RPLE and D-RISE that we used in different regimes of Glauber dynamics and on different Ising model topologies.

The regularization parameter λ has the following functional form

$$\lambda = c_\lambda \sqrt{\frac{\log(n^2/\delta')}{m_u}} \quad (\text{S107})$$

where $1 - \delta'$ is the probability with which we wish to successfully reconstruct the local neighborhood of u . Note that δ' should be related to δ used in the quantifying the success of the whole graph recovery as $\delta' = \delta/n$. We follow an approach similar to that followed in Supplementary material of (Lokhov et al., 2018) to determine the optimal values of c_λ . Our experimental protocol for selecting an optimal value of c_λ on a given Ising model topology is as follows. For a fixed typical values of α and β , we determine m^* for different values of c_λ . The optimal value of c_λ is then defined as the one for which the lowest m^* was obtained. To determine consensus values across topologies, this procedure is repeated on different types of lattices and random regular graphs. Further, as we expect different optimal values of c_λ , the studies are repeated for both the T-regime and M-regime.

The results for the T-regime and M-regime are shown in Figure S1 and Figure S2. We observe that a consensus optimal value of c_λ can be selected across lattices or random regular graphs but not across both topologies. In the T-regime, optimal choice of c_λ for D-RPLE is ≈ 0.05 on lattices and ≈ 0.1 on random regular graphs. In the T-regime, optimal choice of c_λ for D-RISE is ≈ 0.1 on lattices and ≈ 0.45 on random regular graphs. In the M-regime, optimal choice of c_λ for D-RPLE is ≈ 0.05 on lattices and ≈ 0.3 on random regular graphs. In the M-regime, optimal choice of c_λ for D-RISE is ≈ 0.1 on lattices and ≈ 0.7 on random regular graphs. We use these values for producing the scaling results in the Main Text.

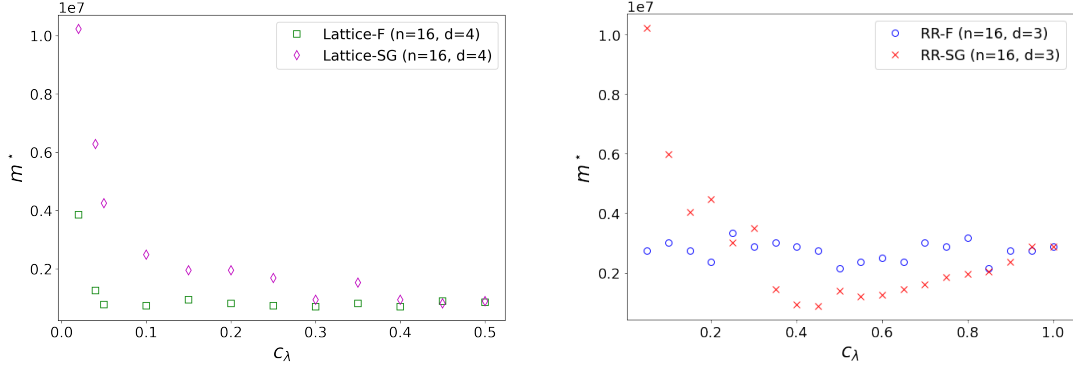
S4. Learning Random Regular Graphs in the M-regime

Here we discuss how structure learning in the M-regime can result in a sample complexity independent of $\beta = \max_{(i,j) \in E} |J_{ij}|$. The central object of our study is the conditional probability distribution in Eq. (2). For simplicity we consider the situation where the magnetic field is zero and we can rewrite this conditional distribution as

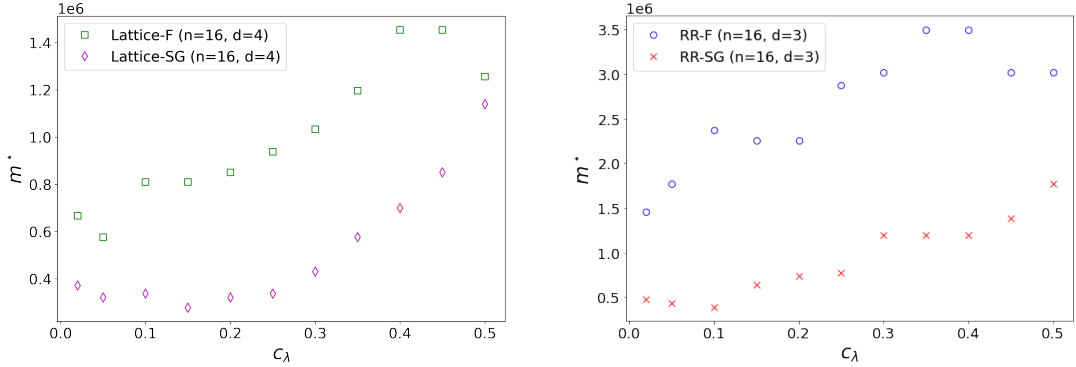
$$p(\sigma_i^{t+1} | \underline{\sigma}^t) = \frac{1 + \sigma_i^{t+1} \tanh \beta \left(\sum_{j \neq i} x_j \sigma_j^t \right)}{2}, \quad (\text{S108})$$

where $x_j = J_{ij}/\beta$ if $j \in \partial i$ and $x_j = 0$ otherwise. In order to analyse the learning problem when β is large, we look at the distribution in Eq. (S108) in the limit where β goes to infinity and we obtain the following expression,

$$\lim_{\beta \rightarrow \infty} p(\sigma_i^{t+1} | \underline{\sigma}^t) = \frac{1 + \sigma_i^{t+1} \text{sign} \left(\sum_{j \neq i} x_j \sigma_j^t \right)}{2}. \quad (\text{S109})$$



(a) D-RISE: Value of $\alpha = 0.4$ for all the graphs. Value of $\beta = 0.8$ on Lattice-F and $\beta = 1.5$ on Lattice-SG. Value of $\beta = 1.2$ on RR-F and $\beta = 1.8$ on RR-SG.

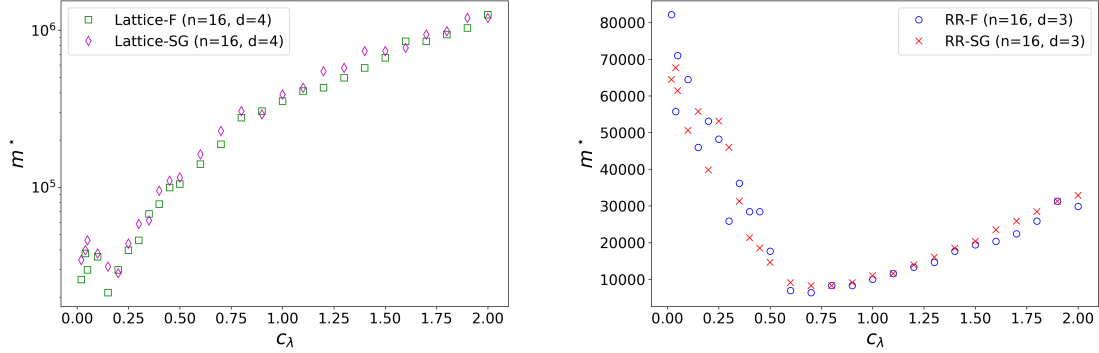


(b) D-RPLE: Value of $\alpha = 0.4$ for all the graphs. Value of $\beta = 0.8$ on Lattice-F and $\beta = 1.5$ on Lattice-SG. Value of $\beta = 1.2$ on RR-F and $\beta = 1.8$ on RR-SG.

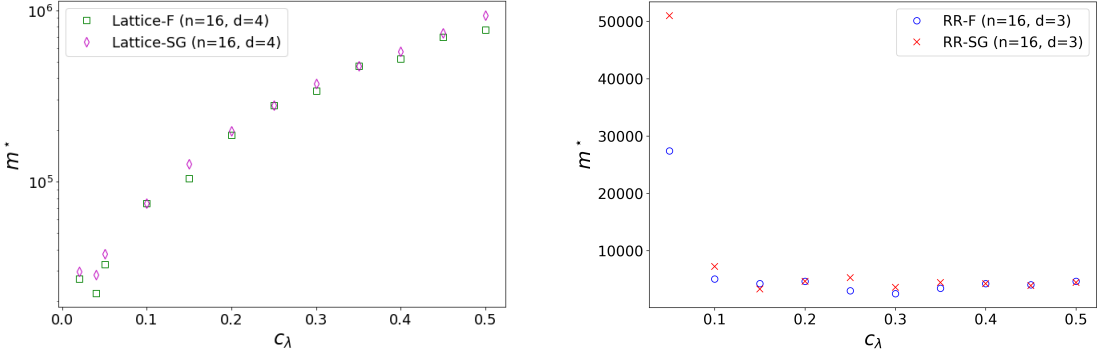
Figure S1: **Empirical selection of c_λ in T-regime** We assess the dependence of the number of samples m^* on the regularization coefficient c_λ for the estimators of D-RISE and D-RPLE for successful structure reconstruction of Ising models of size $n = 16$. The different Ising model topologies considered are: (Lattice-F) ferromagnetic model on a periodic lattice as in Figure 1aA, (Lattice-SG) spin glass model on a periodic lattice as in Figure 1aC, (RR-F) ferromagnetic model on a random regular graph as in Figure 1a, and (RR-SG) spin glass model on a random regular graph as in Figure 1aD.

The form of the conditional distribution in Eq. (S109) implies that the update of σ_i^{t+1} is with probability one equal to $\text{sign}(\sum_{j \neq i} x_j \sigma_j^t)$ whenever $\sum_{j \neq i} x_j \sigma_j^t \neq 0$, otherwise σ_i^{t+1} is updated to -1 or 1 with equal probabilities. We see in the limit of large β that the structure learning problem transforms essentially into the so-called noiseless one-bit compressive sensing problem (Boufounos & Baraniuk, 2008). In noiseless one-bit compressive sensing, we receive $t \in [1, m]$ observations of signs $y \in \mathbb{R}^m$ of the components of an unknown d -sparse vector $\underline{x} \in \mathbb{R}^n$ transformed by a known sensing matrix $A \in \mathbb{R}^{m \times n}$ i.e. $\underline{y} = \text{sign}(A\underline{x})$. The objective in one-bit compressive sensing is to recover the support of \underline{x} just like in our structure learning problem. In order to recover the support of \underline{x} , the number of observations (and the rank of A) has to be at least $m = \Omega(d^2 \ln n / \ln d)$, see (Acharya et al., 2017). The difference between compressive sensing and our structure learning problem lies in the choice of the sensing matrix. While in compressive sensing, the design of the sensing matrix is left to operators, in our case it is imposed by the distribution $p(\underline{\sigma}^t)$ as the rows of our sensing matrix correspond to i.i.d. samples of spin configurations $A_{tj} = \sigma_j^t$.

In the T-regime we expect the Glauber dynamics to mix rapidly and generate samples from the equilibrium distribution of the graphical model. In the limit $\beta \rightarrow \infty$, the equilibrium distribution is supported only by spin configurations whose energies are minimal. The number of such configurations is typically constant with respect to the system size. For example, ferromagnetic models have no more than two states of minimal energy regardless of the number of spins. Therefore, our sensing matrix only contains a fixed number of independent rows and the one-bit compressive sensing problem cannot be solved perfectly as $\text{rank}(A) = O(1)$. It implies that for large β , structure learning with a fixed number of i.i.d. samples



(a) D-RISE: Value of $\alpha = 0.4$ for all the graphs. Value of $\beta = 1.5$ on lattices and random regular graphs.



(b) D-RPLE: Value of $\alpha = 0.4$ for all the graphs. Value of $\beta = 1.5$ on lattices and $\beta = 2.6$ on random regular graphs.

Figure S2: Empirical selection of c_λ in M-regime We assess the dependence of the number of samples m^* on the regularization coefficient c_λ for the estimators of D-RISE and D-RPLE for successful structure reconstruction of Ising models of size $n = 16$. The different Ising model topologies considered are: (Lattice-F) ferromagnetic model on a periodic lattice as in Figure 1bA, (Lattice-SG) spin glass model on a periodic lattice as in Figure 1bC, (RR-F) ferromagnetic model on a random regular graph as in Figure 1b, and (RR-SG) spin glass model on a random regular graph as in Figure 1bD.

from the equilibrium distributions cannot be accomplished.

In the M-regime, however, the distribution $p(\underline{\sigma}^t)$ is uniform and our sensing matrix turns out to be generated from a Bernoulli ensemble with entries equal to -1 and $+1$ at random. Such matrices are known to have a rank m with high probability (Kahn et al., 1995). This renders possible the inversion of the one-bit compressed sensing problem and consequently the possibility to solve the structure learning problem with a number of observations independent of β for β large. However, matrices with random signs do not necessarily lead to an invertible one-bit compressive sensing problem and the invertibility of the problem depends on the hidden vector \underline{x} . For instance, consider the simple four dimensional vectors with different support $u = (1, 1, 1, \epsilon)$ where $|\epsilon| \in (0, 1)$ and $v = (1, 1, 1, 0)$. It is easy to see that for any configurations of $\sigma_i \in \{-1, 1\}$ we have that $\text{sign}(\sum_i \sigma_i u_i) = \text{sign}(\sum_i \sigma_i v_i)$ for the quantity $\sigma_4 u_4 = \epsilon \sigma_4$ has always a smaller magnitude than $|\sigma_1 + \sigma_2 + \sigma_3| \geq 1$. Therefore, structure learning with a fixed number of samples for large β cannot be done for neighborhood of size four and couplings equal to $(\beta, \beta, \beta, \alpha)$, which explains the exponential scaling seen for the lattice instance in Fig. 1b. We have a different story when we consider the three dimensional vector $w = (1, 1, \epsilon)$ with $|\epsilon| \in (0, 1)$. If we take a sensing matrix

equal to $A = \begin{pmatrix} 1 & -1 & 1 \\ -1 & 1 & 1 \\ 1 & 1 & -1 \end{pmatrix}$ when $\epsilon > 0$ or $A = \begin{pmatrix} 1 & -1 & -1 \\ -1 & 1 & -1 \\ 1 & 1 & 1 \end{pmatrix}$ when $\epsilon < 0$, we see that the only three dimensional

vectors x that satisfy the equation $\text{sign}(Ax) = \text{sign}(Aw)$ are those for which $x_1 > 0$, $x_2 > 0$ and $x_3 \cdot \text{sign}(\epsilon) > 0$. This means that the (signed) support of w is recoverable with a sensing matrix from the Bernoulli ensemble. It implies that structure learning with a fixed number of samples for large and even infinite β is possible for neighborhood of size three and couplings equal to (β, β, α) which explains the flat curves seen for the three-regular graphs in Fig. 1b. Based on these considerations, we can extrapolate this behavior in a straightforward manner to graphs with odd and even degree d having

$d - 1$ identical couplings.

S5. Learning dynamics from neural spike trains

In this section, we describe how the relevant dataset from (Prentice et al., 2016) is processed to be used for learning Ising dynamics with D-RISE/D-RPLE in this study. Then, we discuss the statistics of learned model parameters, and compare results obtained with D-RISE and D-RPLE. Finally, we provide details on computation of data moments (such as correlations) from the learned Ising model to assess performance against the dataset.

S5.1. Preparation of neural dataset

The dataset contains spike trains from 152 salamander retinal ganglion cells in response to a non-repeated natural movie stimulus, of which we select spike trains for $n = 42$ neurons over 24s for our application. To obtain a time series of spin configurations over the neurons, we bin the spike trains into 20 ms time bins. The spin $\sigma_i^{(t)}$ of a neuron i in time bin t is set to 1 if it fires at least once in this time bin and -1 otherwise. We thus produce a sequence of 1.2×10^5 spin configurations (also called binary spike words). A segment of the sequence is shown as a spike raster in Figure 2. However, this can't be used directly for learning an Ising model using D-RISE or D-RPLE.

Our learning algorithms require information about the identity of nodes being updated which isn't directly available from the data recorded. The identity of the node being updated at time t is however known when there is some $k \in [n]$ for which the spin of node/neuron k flips in sign i.e., $\sigma_k^{(t+1)} = -\sigma_k^{(t)}$. There maybe more than one such node at time t . However, in Glauber dynamics, only one node is selected for update at time t . We thus only consider samples of spin configurations $\{(\underline{\sigma}^t, \underline{\sigma}^{t+1}, I^{t+1})\}$ for time bins t where I^{t+1} can be directly inferred by searching for nodes which flipped its spin and there is only one such node. It should be noted that the resulting set of 3.2×10^4 samples corresponds to the M-regime with an unknown distribution over the initial spin configurations.

Let us briefly comment on some challenges associated with the dataset preparation procedure that we used, and point out to directions for overcoming these limitations. As we require the identity of the updated nodes for D-RISE/D-RPLE, this requires us to only select samples where a node is observed to be flipped. Otherwise, we wouldn't know a node has been updated or not. The model fit would improve if the node identities weren't required and thus samples were no flips are observed could also be used for estimation. This however requires deriving estimators beyond D-RISE/D-RPLE that is outside the scope of this work, but would be an interesting direction for future studies. The bin size was chosen to be 20ms as this is the expected time scale of persistence of modes in the neural spike trains (Prentice et al., 2016) and was reused. Reducing the bin size decreases the probability of observing a spike or a node activation in that time bin leading to more samples with no updates. Increasing the bin size increases the probability of observing a spike or node activation in the time bin but there may also be more than one spike in the time interval for a given node which is counted only once. Choosing the bin size appropriately ensures that there is enough samples and that the Poisson rate of observation matches closely with the Poisson rate of node updates. We would expect the model fit to overfit if the bin size is too high and be more computationally expensive in the case where bin size is small.

Finally, it would be interesting to go beyond the assumption of Glauber dynamics for constructing an effective model of the data, making use of all available samples that can be costly to get. Possible extensions of our framework include: (i) considering samples with only spin history and thus not requiring identities of updated nodes, (ii) accounting for multiple nodes being updated at the same time e.g., akin to block Gibbs sampling, and (iii) considering more general Markov chain dynamics. We leave these extensions to future work.

S5.2. Statistics of learned model parameters

Ising model parameters learned using D-RISE on the set of samples prepared as discussed in the previous section are shown in Figure S3. If the task is to learn an effective Ising model for explaining the dynamics, these parameter estimates can be used directly. However, if the task is that of a model selection, i.e. learning the network structure of the model, then the following procedure can be used. In the histogram over \hat{J}_{ij} , we observe gaps separating a group of estimated couplings in the vicinity of zero from those with higher intensities in absolute value. We choose the threshold δ to correspond to the first symmetrical gap around zero ($\delta_- = -\delta$ and $\delta_+ = \delta$) that separates these groups. All the coupling parameters $|\hat{J}_{ij}| < \delta$ obtained after structure learning and shown in red in the histogram of Figure S3 would be set to zero. Observing these gaps and ability to choose a clear threshold indicates that the number of samples is sufficient for structure learning.

The resulting \hat{J}_{ij} estimates indicate a low value of β and thus a high effective temperature of the model. Most of the couplings are weak with few strong couplings. This is in agreement with other such studies. The effective Ising model that we learn here from Glauber dynamics can be used for predicting higher order moments of the data and understanding the behavior of this population of neurons. The difference in correlation matrices computed from data assuming the samples are i.i.d. and that respecting time (presented in the Main Text) explain the difference in parameter estimates \hat{J}_{ij} obtained through RISE and D-RISE as visualized in Figure S4. This once again highlights the importance of respecting dynamics and hence time correlations in the data when learning an effective Ising model.

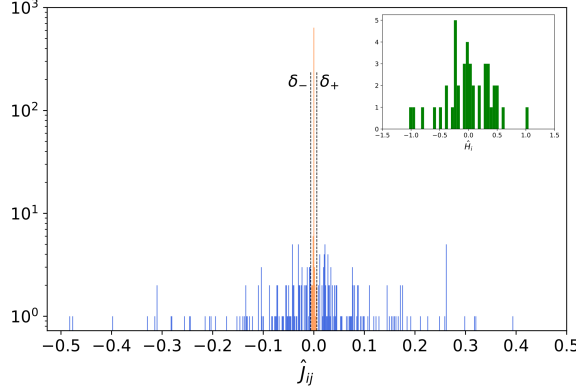


Figure S3: Ising model parameters learned from spike trains over 42 neurons using 3.2×10^4 samples. Significant couplings are in blue and thresholded couplings are in red. Reconstructed fields are in green in a separated histogram.

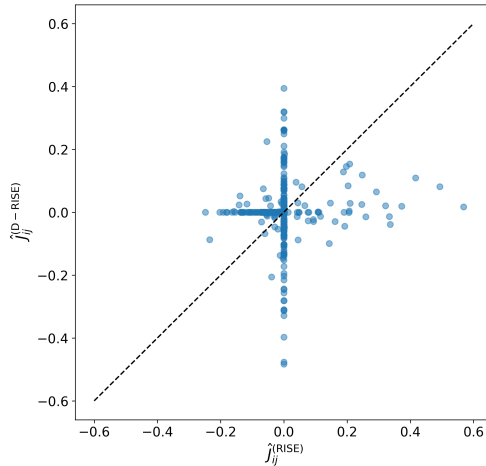


Figure S4: Comparison of Ising model parameter estimates \hat{J}_{ij} obtained through RISE and D-RISE

S5.3. Computation of correlations

To assess the performance of the learned Ising model, it is common to compare predicted correlations from the model against the data. Here, we obtain predicted correlations by computing correlations on a dataset simulated using the learned Ising model under the M-regime and running Glauber dynamics. We now explain how this simulated dataset is constructed.

We note that the covariance of interest (including the corresponding probabilities) is given by

$$\text{Cov}(\sigma_i^0, \sigma_j^1) = \mathbb{E}_{p(\sigma_j^1 | \sigma_i^0, I^1) p(\sigma_i^0) p(I^1)} [\sigma_i^0 \sigma_j^1] - \mathbb{E}_{p(\sigma_i^0)} [\sigma_i^0] \mathbb{E}_{p(\sigma_j^1 | \sigma_i^0, I^1)} [\sigma_j^1] \quad (\text{S110})$$

We note from the above expression that the resulting covariance not only depends on the Ising model dynamics which explains $p(\sigma_j^1 | \sigma_i^0, I^1)$ but also the initial distribution over spin configurations $p(\sigma_i^0)$ and the probability of a node being chosen for update $p(I^1)$. In order to ensure we can compare the predicted covariance from the Ising model against that from data, we use the same $p(\sigma_i^0)$ and $p(I^1)$ as in the experimental dataset. Additionally, we note that the spin configurations in the experimental dataset only contains flipped spin configurations which also needs to be respected.

Thus, we construct the simulated dataset by running Glauber dynamics on the M-regime using the same $p(\sigma^0)$ and $p(I^1)$ as from the experimental dataset, and only including those σ^1 where there is a flip in the sign of node given by I^1 . Moments are then computed on this simulated dataset using the usual estimators for population means, covariances, correlations, etc., from the samples.